

Magnetically Enhanced Microflow Cytometer for Bead-based Immunoaffinity Measurements in Whole Blood Samples



Scientific thesis for the attainment of the academic degree
Master of Science (M.Sc.)
of the Department of Electrical and Computer Engineering
at the Technical University of Munich.

Supervised by Dr.-Ing. Mathias Reisbeck
Prof. Dr. rer. nat. Oliver Hayden

Submitted by Johann Alexander Brenner
Weisbergerstraße 5a
85053 Ingolstadt
03662733

Submitted on December 4th, 2020 at Munich

Contents

1 Theory	1
1.1 Microfluidics	1
1.1.1 Incompressibility of Fluid Flows	1
1.1.2 Flow and Shear in Microchannels with Viscous Fluids	2
1.1.3 Force Equilibrium of Microbeads	4
1.1.4 Rolling Motion and Surface Interaction of Beads.....	10
1.2 Surface Chemistry	15
1.2.1 Surface Oxidation Methods.....	15
1.2.2 Silane Chemistry	18
1.2.3 Carbodiimide Crosslinker Chemistry	19
1.2.4 The Biotin-Avidin-System	21
1.3 Magnetoresistive Sensing	22
List of Abbreviations.....	27
List of Figures	30
List of Tables	31
Bibliography	33
Statement	49

1. Theory

The main measurement principle of a microfluidic channel in connection with a giant magneto resistance (GMR)-Sensor has been already described and characterized exhaustively by Helou [1], Reisbeck [2] and others.[3, 4] Therefore, this theoretical part will focus on (bio-)physical aspects of a cell rolling motion inside a microfluidic channel and surface modification chemistry.

1.1. Microfluidics

1.1.1. Incompressibility of Fluid Flows

The main experiments of this work were carried out in microfluidic environments, which exhibit favorable properties compared to common macrofluidic systems. From a fluid-mechanical standpoint, shrinking the scales makes interfacial as well as electrokinetic phenomena much more significant, and reduces the importance of pressure and gravity.[5] However, electrodynamics, chemistry and fluid dynamics are inextricably intertwined, so that fluid flow can create electric fields (and vice versa), with a degree of coupling driven by the surface chemistry. Many of the resulting phenomena arise or can be explained by the conservation of mass described by the continuity equation (Eq. 1.1) and the conservation of momentum described by the Cauchy-Momentum equation (Eq. 1.4) and the resulting Navier-Stokes equation(Eq. 1.8).

$$\frac{\partial}{\partial t} \iiint \rho \, dV = - \iint \rho \mathbf{u} \cdot \vec{n} \, dA \quad 1.1$$

$$\nabla \cdot \mathbf{u} = 0 \quad 1.2$$

$$\frac{\partial}{\partial t} \iiint \rho \mathbf{u} \, dV = - \iint \rho \mathbf{u} \mathbf{u} \cdot \vec{n} \, dA + \iint \boldsymbol{\tau} \cdot \vec{n} \, dA + \iiint \sum_i \mathbf{f}_i \, dV \quad 1.3$$

$$\rho \frac{\partial \mathbf{u}}{\partial t} + \rho \mathbf{u} \cdot \nabla \mathbf{u} = \nabla \cdot \boldsymbol{\tau} + \sum_i \mathbf{f}_i \quad 1.4$$

$$1.5$$

The foremost assumption in fluid dynamics is termed “incompressibility”, when density gradients are negligibly small to assume a uniformity thereof. This leads to a significant

simplification of the conservation equations, because any transfer from kinetic to internal energy can be ignored.¹ This equation states that the mass of a control volume (in this case the volume integral over the density (ρ)) can only change by the mass flux over its unit outward normal (\vec{n}) transported by the flow field (\mathbf{u}). For constant ρ the mass does never change over time. This finding and the application of Gauss's theorem yields the conservation of mass in an incompressible fluid. (Eq. 1.2)

1.1.2. Flow and Shear in Microchannels with Viscous Fluids

The final equation and Gauss's theorem can now be applied to the conservation of momentum relation. (Eq. 1.3) Integration yields then the Cauchy momentum equation which states that any change in momentum inside a control volume ($\rho \frac{\partial \mathbf{u}}{\partial t}$) is caused by convective transport for or to the volume ($\rho \mathbf{u} \cdot \nabla \mathbf{u}$), surface stresses ($\nabla \cdot \boldsymbol{\tau}$), and the volumetric net body forces (\mathbf{f}_i) such as gravity or electrostatics.

Hereby, the surface stress surface stress tensor ($\boldsymbol{\tau}$) can be further decomposed into the pressure stress tensor ($\boldsymbol{\tau}_{pressure}$) and viscous stress tensor ($\boldsymbol{\tau}_{viscous}$) as shown in the equations Eq. 1.6. Characteristically, the pressure related contributions act normal and independently from \mathbf{u} whereas viscous forces act normal and tangential, and are dependent on \mathbf{u} . The $\boldsymbol{\tau}_{pressure}$ can therefore be expressed by a scalar pressure acting in every spatial dimension which is spanned by the identity.

The viscous stresses however can not be described by a continuum equation but only by a constitutive relation of atomistic processes. The underlying fundamental model of Newton's mechanics assumes that dynamic viscosity (η) is neither dependent on any velocity nor on the strain rate. Therefor, fluids which satisfy this condition are called "Newtonian fluids". Omitting special cases such as shear-thinning, -thickening or complex colloidal fluids such as undilute blood, η is the scalar proportionality that relates the strain rate to surface stress.[5] This is captured in the equation $\boldsymbol{\tau}_{viscous} = 2\eta\boldsymbol{\epsilon}$. Thereby, shear stress tensor ($\boldsymbol{\epsilon}$) is part of the decomposition of an unidirectional flow field. It resembles on the one hand side any stretching or squeezing of fluid by "extensional"

¹ For sake of completeness, it should be mentioned that viscous forces can also transfer energy irreversibly to internal energy. However, they are inversely proportional to the system's size, and hence omitted.

strain and on the other hand side “shear” strain which is responsible for skewing.[5]

$$\boldsymbol{\tau} = \boldsymbol{\tau}_{viscous} + \boldsymbol{\tau}_{pressure} = 2\eta\boldsymbol{\epsilon} - p\mathbf{I}_{3\times 3} \quad 1.6$$

$$\nabla \cdot \boldsymbol{\tau}_{viscous} = \nabla \cdot 2\eta\boldsymbol{\epsilon} = \nabla \cdot \eta\nabla\mathbf{u} \stackrel{\text{only if } \eta \text{ uniform}}{=} \eta\nabla^2\mathbf{u} \quad 1.7$$

$$\underbrace{\rho \frac{\partial \mathbf{u}}{\partial t}}_{\text{Transient}} + \underbrace{\rho \mathbf{u} \cdot \nabla \mathbf{u}}_{\text{Convection}} + \underbrace{-\nabla p}_{\text{Pressure}} + \underbrace{\eta \nabla^2 \mathbf{u}}_{\text{Viscous}} + \underbrace{\sum_i \mathbf{f}_i}_{\text{Body Forces}} = 0 \quad 1.8$$

The divergence of $\boldsymbol{\tau}_{viscous}$, as used in the incompressible Cauchy momentum equation (Eq. 1.4), can then be simplified with Eq. 1.7 further by taking advantage of the anti-transpose symmetry of the flow field. If η is also uniform respectively isotropic across the channel, the divergence is completely independent of the scalar viscosity. Applying all assumptions to the Cauchy momentum equation (Eq. 1.4) yields as final result the Navier-Stokes-Equation (NSE). (Eq. 1.8)

However, the NSE has no analytic solution yet and can in consequence only solve defined boundary problems. The two most common boundary conditions herefore are the “no-penetration condition” ($\mathbf{u} \cdot \vec{n} = 0$) and the “no-slip condition” ($\mathbf{u}_t = \mathbf{u} - (\mathbf{u} \cdot \vec{n}) \vec{n} = 0$), which state that the normal and tangential components of fluid velocity are per definition zero at motionless, impermeable walls.

Besides these conditions, many problems arise due to turbulent flow and therefor transient effects. Mathematically, this can be avoided by simply neglecting the time-dependent term in the NSE. Also, it can be argued from a systematic point of view that, for viscosity-dominated flows, fluid moves in isoplanar “lamina”. In experimental observations, these laminar flows then proved to be stable to perturbations thus steady.

$$Re = \frac{\text{fluid density} \cdot \text{velocity} \cdot \text{size}}{\text{viscosity}} \quad 1.9$$

In a first order approximation, the dimensionless Reynolds number (Re), which compares the inertia to viscous forces, allows a qualitative prognosis about the flow regime. (Eq. 1.9) If it results below a threshold of 2300, laminar flow can be assumed in Hagen-Poiseuille flows. This holds true for the utilized microfluidic with the dimensions $12\,000\,\mu\text{m} \times 700\,\mu\text{m} \times 150\,\mu\text{m}$ ($l \times w \times h$) and aqueous buffer solutions, where the channel width considered as characteristic length l . Hence, several fluidic phenomena such as deter-

ministic pathlines as well as simplifications of the NSE can be exploited in the present system.

In the model case of a flow through a rectangular channel, no analytical solution of the NSE exists, but a Fourier Series expansion if the width is larger than height of a channel as shown in Bruus [6].² Equation Eq. 1.10 determines the magnitude of the flow field parallel to the pressure gradient in relation to the horizontal dimension y and vertical dimension z with respect to the channel dimensions height h and width w . An integration over the flow field in the channel cross section yields the flow rate (Q). (Eq. 1.11)

$$\mathbf{u}_x(y, z) = \frac{4h^2\Delta p}{\pi^3\eta l} \sum_{n,odd}^{\infty} \frac{1}{n^3} \left(1 - \frac{\cosh(n\pi\frac{y}{h})}{\cosh(n\pi\frac{w}{2h})} \right) \sin(n\pi\frac{z}{h}) \quad 1.10$$

$$Q = \int_{-\frac{1}{2}w}^{\frac{1}{2}w} \int_0^h u_x(y, z) dz dy \approx \frac{h^3 w \Delta p}{12\eta l} \left(1 - \frac{h}{w} \right), \text{ for } h < w \quad 1.11$$

1.1.3. Force Equilibrium of Microbeads

Although microfluidic systems mostly operate in a low inertia regimes as specified by low Re , the force equilibrium $\sum_i \mathbf{F} = 0$ and subsequently the velocity of any particle in the fluid stream is influenced as it moves closer to the boundaries. Several models have already been implemented with a part of the mentioned forces. Lee and Balachandar [7] compared the importance translation, rotation and shear forces.[8] evaluated cell rolling characteristics and Wu and Voldman [9] proposed a model for bead-based immunoassays in microfluidics. Therefore, an overview over all (inter-)acting forces shall be given here.

$$Re_{particle} = \frac{r^2}{\frac{2wh}{w+h}} Re \quad 1.12$$

Additionally to the channel Reynolds number Re , describing the ratio between inertial force and viscous force of fluid in a flow, Di Carlo et al. [10] proposed a particle Reynolds

² The equation Eq. 1.10 shows that height deviations can have prominent influence on a channel velocity simulation as it is proportional to h^2 . Further, the flow rate depends even on h^3 .

number ($Re_{particle}$) considering the size ratio of particle to channel. When $Re_{particle} \ll 1$ particles are subjected to the dominant viscous drag to follow fluid streamlines. In the contradictory case, inertia becomes prominent. However, on increasing $Re_{particle}$ to the order of 1, inertial lift forces become dominant and lateral migration of particles across streamlines becomes visible. For a micrometer sized bead and a channel as mentioned in Section 1.1.2, the pre-factor is in the range of 1×10^{-5} hence viscous drag outweighs inertial lift of a particle.

Stoke's Drag

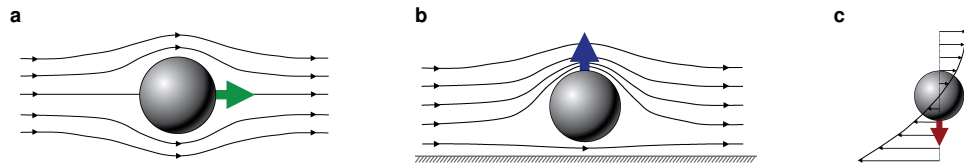


Figure 1: Particle Drag and Lift Behavior

(a) Bulk Drag: Force acts on a particle caused by the displacement of fluid stream lines. (b) Wall-lift Drag Force: In a special case of drag, where streamlines cannot be displaced further, a pressure gradient forms in front of the sphere. This forces a motion directed perpendicularly from the wall. (c) Shear-induced force: The curvature of the flow profile exhibits a translation and rotation due to inhomogeneously distributed shear on the surface.[11]

The foremost force to actuate particles inside a microfluidic channel is Stoke's drag force (\mathbf{F}_{drag}). (Eq. 1.13) It originates from viscous fluid moving past the sphere surface, where a slip condition has to be applied. The fluid therefor has to displace its elements in front of the movement direction.[12] A particle with the surrounding streamlines is depicted in Fig. 1a for the bulk case and in Fig. 1c for adjacent walls.

$$\mathbf{F}_{drag,wall} = -6\pi\eta r \bar{\mathbf{u}} K \quad 1.13$$

$$K = \frac{4}{3} \sinh \alpha \sum_{n=0}^{\infty} \left(\frac{n(n+1)}{(2n-1)(2n+3)} \cdot A \right) \quad 1.14$$

$$\alpha = \cosh^{-1} \frac{z}{r}, \quad 1.15$$

$$A = \frac{2 \sinh((2n+1)\alpha) + (2n+1) \sinh 2\alpha}{(2 \sinh((n+0.5)\alpha))^2 - ((2n+1) \sinh \alpha)^2} - 1 \quad 1.16$$

$$K_{approx} = \frac{24}{Re} * \left(\frac{1 + \frac{2}{3}\lambda}{1 + \lambda} \right), \text{ with } \lambda = \frac{\eta_{fluid}}{\eta_{particle}} \quad 1.17$$

$$v_z = \frac{3}{64} Re_s \mathbf{u}_s = \frac{3}{64} \frac{\rho_{fluid} r \mathbf{u}_s}{\eta} \mathbf{u}_s, \left(\frac{\rho_{fluid} l_w \mathbf{u}_s}{\eta} \right) \ll 1 \quad 1.18$$

$$\omega = \frac{3\mathbf{u}}{32r} \left(\frac{r}{l} \right)^4 \left(1 - \frac{3}{8} \frac{r}{l} \right), \text{ for } \left(\frac{r}{l} \right)^2 \ll 1 \quad 1.19$$

In the proximity of a channel wall, where no fluid can be displaced further, a correction

factor was determined by Happel and Brenner [13] that approximates drag in a perpendicular direction.(Eq. 1.14) Repulsion velocity can then be defined by the Reynolds number calculated with a sedimentation velocity (\mathbf{u}_s) if the particle center has a distance $l_w \ll 1$ from the wall.[14, 15] A phenomenological approximation of the correction factor yields equation Eq. 1.17, when viscosity dominates the difference. Adapted to an example, a spherical air-bubble inside a water flow feels only 67.4% of the drag by surrounding fluid.

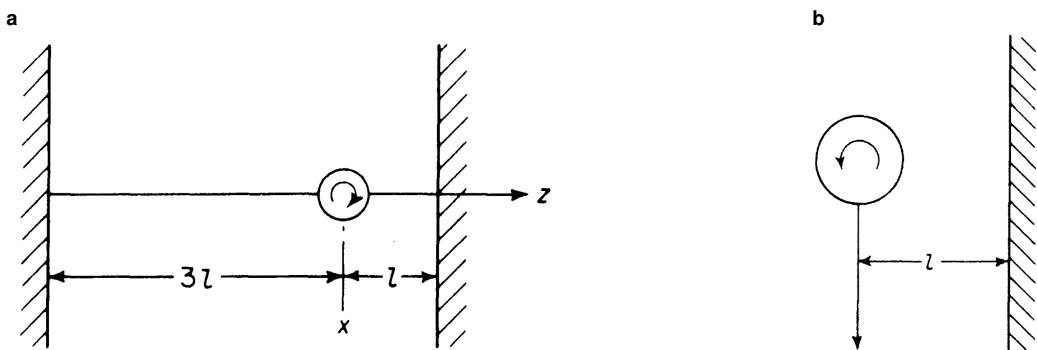


Figure 2: Particle Rotation Behavior

(a) Direction of rotation of a sphere settling in eccentric position between parallel walls. (b) Direction of rotation of a sphere settling in the presence of a single plane wall far from the other side.[10]

The considerations of Stoke's drag force above were limited for only linear translation cases. However, fluid drag also imposes a torque on particles. Happel and Brenner [13] mention an experimentally determined formula in 1.19 to calculate a drag-related angular rotation frequency (ω). Counter-intuitively, the direction of rotation in the bulk fluid (Fig. 2a) is opposite than from the rotation direction near or touching the wall (Fig. 2c). This can be explained by a complex superposition of tangential components from later mentioned forces and will not be explained to any more extent here.

Gravity and Buoyancy

On every mass in our environment acts gravity (\mathbf{F}_{grav}) to pull it along its gradient. In a medium, however, it is balanced by the displacement of the same in the counter-direction called buoyancy ($\mathbf{F}_{buoyancy}$). As a microparticle made from a co-polymer - especially when it is magnetic - has a significantly higher density than water, \mathbf{F}_{grav} (Eq. 1.21) outperforms $\mathbf{F}_{buoyancy}$ (Eq. 1.20), which in term causes a particle to sink to

the channel floor.

$$\mathbf{F}_{buoyancy} = -\frac{4}{3}\pi r^3 \rho_{fluid} g \quad 1.20$$

$$\mathbf{F}_{gravity} = +\frac{4}{3}\pi r^3 \rho_{particle} g \quad 1.21$$

Magnetic Force

The - during the course of this thesis - strongest acting force is exhibited by the magnetic flux density (\mathbf{B}), which acts on paramagnetic particles with a magnetic dipole moment (\mathbf{m}). When an external magnetic field is non-uniform, there will be a magnetic force (\mathbf{F}_{mag}), proportional to the magnetic field gradient, acting on the magnetic dipole moment.(Eq. 1.24) For particles that carry magnetite or similar ferrimagnetic material in their polymer matrix or shell, the magnetic moment can be inferred by the relation $\mathbf{m} = MV$, where the magnetization (M) of a volume V is known. However, the more exact approach is a comparison of magnetic susceptibilities (χ) as described in Eq. 1.22. Consequently, if the particle susceptibility is greater than the fluid's, a microbead will move towards the field maximum. Calculated for an 8 μm bead with 3.8 A m^2 saturation magnetization, \mathbf{F}_{mag} results in $\sim 45 \text{ pN}$ for a field gradient of 5 T m^{-1} .

$$\mathbf{F}_{mag} = \frac{V_p (\chi_p - \chi_f)}{\mu_0} (\mathbf{B} \cdot \nabla) \mathbf{B} \quad 1.22$$

$$\mathbf{F}_{dipole} = (\mathbf{m} \cdot \nabla) \mathbf{B} = -\nabla \mathbf{E}_{dipole} \quad 1.23$$

$$\mathbf{E}_{dipole} = \sum_{i=1}^n \frac{\mu_0}{4\pi r_i^3} \left(\mathbf{m}_i \cdot \mathbf{m}_{ref} - \frac{3}{|\mathbf{r}_i|^2} (\mathbf{r}_i \cdot \mathbf{m}_i) (\mathbf{r}_i \cdot \mathbf{m}_{ref}) \right) \quad 1.24$$

Additionally, the magnetic beads interact with each other according to the dipolar interaction, where a reference bead with magnetic momentum \mathbf{m}_{ref} at distance \mathbf{r}_{ref} feels the force of all surrounding particles. (Eq. 1.24)

Electrostatic Interaction

The microchannel, as well as a particle in it, carries an electrical double layer on the surface, due to present surface charges. The net charge acquired by the particles can be computed by integrating the particles' surface charge densities over their surfaces as described by Gauss's Law. However, as Coulomb's force (\mathbf{F}_{el}) on charge q_1 is square

dependent of the distance from the secondary charge q_2 at the respective locations \mathbf{r}_1 , \mathbf{r}_2 . (Eq. 1.25) This, and the fact that the surface net charge in a buffer solution is insignificant, lead to the assumption that \mathbf{F}_{el} plays a minor role in this force equilibrium.

$$\mathbf{F}_{el} = \frac{q_1 q_2}{4\pi\epsilon_0} \frac{\mathbf{r}_1 - \mathbf{r}_2}{|\mathbf{r}_1 - \mathbf{r}_2|^3} \quad 1.25$$

Magnus Lift Force

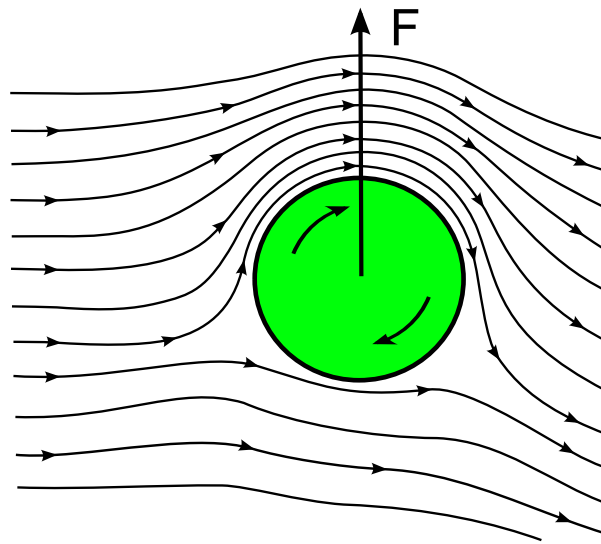


Figure 3: Magnus Effect on a Particle in Laminar Flow

The intrinsic rotation of a particle inside a laminar flow field causes a pressure gradient to the side whose tangential rotation vector is parallel to the stream lines.

The Magnus lift force (\mathbf{F}_{magnus}) is a rotation-induced variable as a result of the pressure difference induced by streamline asymmetry.[16] For a spinning particle in a fluid as shown in Fig. 3, the streamline density and therefore the pressure on the one side of the particle is lower than the pressure on the other side. The main driver of this effect is again the no-slip boundary, where fluid on the front side of the particle is dragged down whereas the fluid on the bottom side is slowed down. As a result, this leads to a lift force perpendicular to the flow direction.

$$\mathbf{F}_{magnus} = \frac{1}{8}\pi r^3 \rho_{fluid} (\mathbf{u} \times \boldsymbol{\Omega}) \quad 1.26$$

Saffman Lift Force

When the rotation speed of a particle in shear rate direction is much greater, $\Omega > 12\nabla\mathbf{u}$, for a freely rotating particle Saffman lift force ($\mathbf{F}_{saffman}$) will begin to act. Depending on the interaction of slip velocity and shear, it will counteract any movement to the planar surface. Hence, at high gradients the center of rotation causes a shift to the maximum shear.

Scaling with the ω , it will generally be at least one order of magnitude larger than Magnus force. Especially for electrically or magnetically actuated particles, shear-induced lift force (\mathbf{F}_{shear}) is more relevant in the case of non-neutrally buoyant spheres.[16]

Shear-induced Lift Force

This \mathbf{F}_{shear} particles to migrate toward walls until the wall lift force repels and balances it. In contrast, if the curvature of \mathbf{u} is zero, it collapses to a simple shear flow. Then the pressure will be higher on the far from the center pushing particles to the centerline of channel. As shown in Fig. 1e the magnitude of \mathbf{u} in particle is much higher on the top side of particle than that on the bottom side, due to the parabolic nature of velocity profile. Similar to Saffman force, the dissymmetry of relative velocity causes a lower pressure on the wall side, generating a shear gradient lift force which is opposite to the Saffman force.[16]

$$\mathbf{F}_{shear} = \frac{81.2}{4}(\mathbf{u} - \mathbf{u}_p)r^2 \sqrt{\frac{\rho_{fluid}}{\eta}} \nabla \mathbf{u} \quad 1.27$$

Deformability-Induced Lift Force

Although solidity can assumed in the first order to the study of hydrodynamic behaviour of particles in a microchannel, cells and vesicles are not rigid but deformable. The deformability will induce an additional lift forces on the particles, which is perpendicular to the main streamline, and it is subjected nonlinearities caused by the matching of velocities and stresses at the deformable particle interface.

$$\mathbf{F}_{deformation} = \mu U r \left(\frac{r}{H} \right)^2 \frac{l_w}{H} f(\lambda) \quad 1.28$$

$$f(\lambda) = \frac{16\pi}{(\lambda+1)^3} \left[\frac{11\lambda+10}{140} (3\lambda^3 - \lambda + 8) + \frac{3}{14} \frac{19\lambda+16}{3\lambda+2} (2\lambda^2 - \lambda - 1) \right] \quad 1.29$$

For example deformability-induced lift force can be used to separate and enrich malaria-infected red blood cell (RBC) from normal healthy RBC for the diagnosis of malaria. The parasite releases proteins that trigger the cross-linking of the spectrin network of the membrane, thus increases the rigidity of the infected cells.[17] Mach and Di Carlo [18] reported a parallelized microfluidic device that passively separates pathogenic bacteria from the diluted blood by the use a unique differential transit time due to channel height differences which in turn caused size-dependent inertial lift forces to obtain cell separation.

Fåræus and Fåræus-Lindquist Effect

Often confused, the Fåræus and Fåræus-Lindquist effect constitute two different hemodynamic properties relevant for microfluidics with blood samples. Whereas the Fåræus effect states that RBCs are depleted in the wall regions of capillaries (due to the lift forces mentioned before), the Fåræus-Lindqvist effect describes the behavior of blood to decrease its viscosity in narrow channels.[19, 20] Thereby, the latter effect is not solely driven by the first, but also the Segré-Silberberg effect, who discovered that for neutrally buoyant particles an equilibrium at exact $0.6r$ from a tubing center forms.[21] To model this effect, Chebbi [22] developed a cell-free marginal layer model.

1.1.4. Rolling Motion and Surface Interaction of Beads

A nice intro goes here

Contact Area of a Sphere and Flat Surface

Once the acting forces brought the bead in contact with a wall or the channel bottom, it starts to move forward in a rolling motion. In a simple model, rolling on a plane without slipping is constrained by a sphere's translation ($\mathbf{F}_{||}$, \mathbf{F}_{\perp}), rotation (ω), and shear. Nevertheless, due to the rigid nature of the sphere, any drag will be omitted in further models.[23] The no-slip boundary condition has to be applied also here by the require-

ment that the points of the sphere momentarily in contact with the plane are at rest. However, rolling contact problems are dynamic because the contacting bodies are continuously moving with respect to each other. The contact patch in a sliding problem continuously consists of the same particles. In contrast, particles enter and leave the contact area during rolling. Moreover, in a sliding problem the surface particles in the contact patch are all subjected the same tangential shift everywhere, whereas in a rolling problem the surface particles are stressed in different ways. During rolling, they are free of stress when entering the contact, then stick to a particle of the opposing surface, and are strained by the overall motion difference between the two bodies, until the local traction bound is exceeded and local slip sets in.[24]

In a real world, pressing two bodies with rough surfaces against each other limits the contact between the two bodies to a value, which is much smaller than the nominal contact area. Additionally, on natural and engineering surfaces Lennard-Jones potential, wetting, and molecular interactions start to play a role on the spectated microscale.[25]

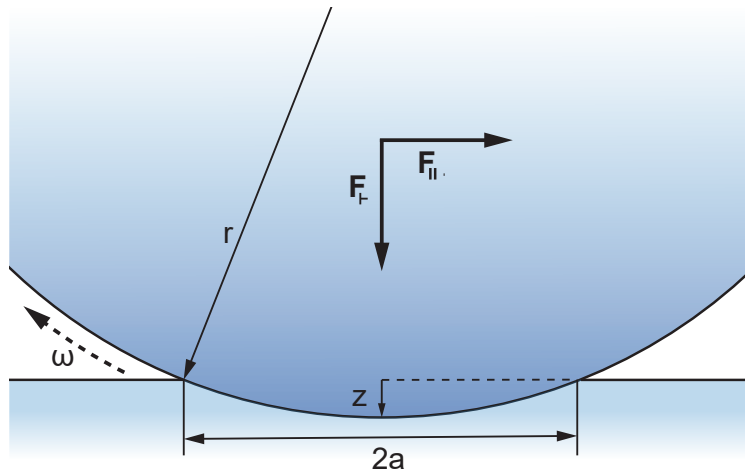


Figure 4: Rolling Mechanics of a Sphere

Penetration model of a sphere with radius r adapted from Azad and Featherstone [25] and Waters and Guduru [26]. The top body moves into the elastic bottom body for an approach (z) and a contact area πa^2 .

In reality, with elastic effects taken into consideration, a different situation occurs. If an elastic sphere is pressed onto an elastic plane (ideally of the same material), both bodies deform and a Hertzian pressure distribution arises. The center of the sphere is moved down by an approach (z) as shown in Fig. 4 that can also be described as “maximum penetration distance”. It can now be calculated that the normal contact area between the bodies follows $A_{contact} = \pi a^2 = \pi (2rz - z^2) = 2\pi rz \left(1 - \frac{z}{2r}\right)$. Assuming that $z \ll 2r$ and considering that $A_{contact}$ must be zero for all $z < 0$, the following

equation for the contact area arises. (Eq. 1.30) The spherical contact surface can be calculated analogous Eq. 1.31.[25]

$$A_{contact} = 2\pi r z, \text{ for } z \geq 0 \quad 1.30$$

$$S_{contact} = \pi r(2z + d) = \pi r(2z + \sqrt{2rz}), \text{ for } z \geq 0 \quad 1.31$$

For a $8\mu\text{m}$ microbead and a penetration depth z of 100 nm this yields for example an interaction with 6.84% of the total sphere and a total area of $13.753\mu\text{m}$. Several methods and experiments have already been developed in the literature to measure the resulting friction and penetration parameters. A general model of a sphere in contact with a wall was optimized by Krishnan and Leighton [27]. Experimentally, Waters and Guduru [26] developed a microtribometer in PDMS to evaluate adhesion properties and validate their model's predictions.

Protein interaction during Rolling

In the attempt to mimic rolling adhesion on vascular surfaces which is the first step in recruiting circulating leukocytes and other cells into the tissue, protein-protein-interactions as driver for microbead motions have been studied extensively in this thesis. Statistically, a cell flowing near the vessel wall is able to attach if its adhesion receptors contact ligands on the wall. Bond formation, anyhow, involves distinct steps: transport, which brings two molecules into close proximity, and reaction, during which the molecules dock. Faster cell velocity produces more collisions but also limits the interaction time between interaction molecules. Thus, the relative timescales for transport and docking affect the efficiency of tethering a flowing cell to the surface.[28]

For these properties, Dembo et al. [29] developed a detailed physical description of membrane adhesion and detachment kinetics. Wu and Voldman [9] then proposed an integrated model for bead based rolling mechanisms under the influence of protein interaction. The key for interaction thereby is the specific *affinity* respectively *avidity* of the protein and its ligand. In general, high-affinity ligand binding results from greater attractive ligand-receptor-forces and results in a higher tenancy of the receptor. However, lifetime of a formed complex does not correlate. The net ligand affinities are unitized by

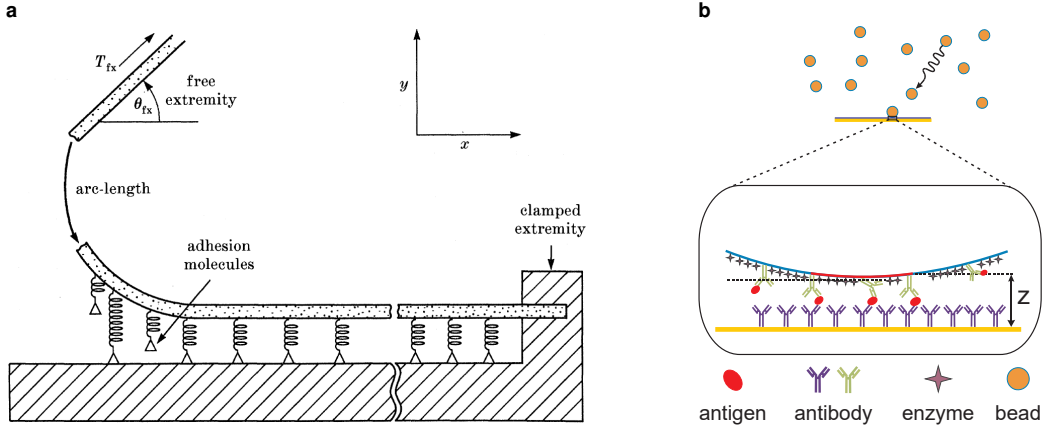


Figure 5: Membrane Adhesion and Detachment Models

a Adhesion Model after Dembo et al. [29]: Every interaction is viewed as spring-damper-model in superposition. **b** Surface Coverage Assay Model: In a stochastic approach, analyte molecules and their interactions are modeled between a planar and a spherical surface. Adapted from Wu and Voldman [9]

the dissociation constant (K_d), which relates the reverse reaction rate ("the dissociation of the bond") to the forward reaction rate ("the formation of the bond"). Therefore high-affinity results in low K_d .

On a bead and microchannel surface, however, not only one but multiple protein-ligand complexes are formed and dissociated simultaneously. This is described by *avidity*. Through single binding events elevate the likelihood of other interactions, avidity is not relating the sum of its ingredient affinities but can rather be seen as the combined effect of all affinities participating in the biomolecular interaction.[30]

Main factor for the method in this thesis is now the critical tension (T_{crit}). A particle - cell or bead - flowing in a low-Reynolds number environment, experiences a \mathbf{F}_{shear} and a torque rotation vector (Ω), which both reach maximum when the particle stops. For this, the two forces must be counteracted by a tensile force on the adhesive bonds and a compressive force at the bottom of the particle. Moreover, these forces affect the forward and reverse reaction rates of the bonds. Any rolling motion stops when the adhesion can withstand the force required to counteract the maximal other forces. After break-up of these bonds the particle begins to accelerate downstream until a newly formed bond develops sufficient strength. Consequently, the intrinsic mechanics of these bonds and how their respective off-rates act under force critically determines whether and how bead roll in a flow field.[28]

There exist two distinct bond types that take effect during the above processes: *Slip*

bonds are linkages whose lifetime is shortened to some extent by external force whereas *catch bonds* lock more tightly upon deformation stress. In biological systems, for example selectines, another effect arises. Upon increasing external stress, bond lifetimes with the ligand are first prolonged until a threshold where bonds are starting to decease. In contrast, if an antibody is the ligand only slip bonds are formed in response to force.[31, 32] By studying the exact forces acting on a particle-protein interaction system affinity based sorting and ultrasensitive assays can be established.[33]

1.2. Surface Chemistry

Introducing biological samples, such as peripheral whole blood and -plasma, into microsystems needs careful consideration of surface modification compared to buffered samples of adjusted pH containing cells or polymeric beads. Blood-material contact most often initiates surface-mediated reactions that lead to cell activation, blood clotting or biofilm formation.[34, 35] In order to minimize unspecific interactions on surfaces, most contact faces are passivated with chemically and biologically inert materials or even composed entirely from it. In any use case, where a surface has to be functionalized with biomolecules, the intrinsic inertness then requires specialized methods for permanent and reproducible adhesion.[36, 37]

Molecules can be immobilized through various mechanisms on surfaces to achieve a biological or chemical functionality. The most simple is physisorption. Here, a biomolecule is bonded only by weak elektrostatic, van-der-Waals or dipole-dipole interaction with a adsorption enthalpy below 50 kJ mol^{-1} .[37] In contrast, this yields fast reaction rates, because no activation energy has to be overcome. Although a large number of molecules can be captured with this method, several drawbacks have been identified.[38–41] Therfore, most functionalization approaches rely on chemisorption where molecules are covalently bound to a surface. Due to the higher activation energy barrier this bonding mechanism works slower in comparison to physisorption, though higher temperatures or catalysts can promote an equilibrium. One of the most well-known strategies to bring reproducible thin films on surfaces is the formation of self-assembled monolayers (SAMs) where a dense layer of single molecules with high internal order forms upon dipping into a surface-active substance.[42]

1.2.1. Surface Oxidation Methods

Modifying a surface with functional silanes, requires oxidized sites, for example $-\text{OH}$ (hydroxyl) resp. $\text{Si}-\text{OH}$ (silanol) groups. In order to increase the presence of those reactive groups on substrates, various activation methods such as a mixture from hydrogen peroxide with excess of sulfuric acid (piranha) and sulfuric acid (H_2SO_4), oxygen gas (O_2) - plasma treatment or an hydrofluoric acid (HF) dip can be chosen.[43]

Critical for any surface engineering is the internal structure and in consequence the binding energies of the surficial groups. The three mainly used substrates in this work,

glass, poly(dimethyl siloxane) (PDMS) and silicon nitride (Si_3N_4), contain highly conserved, homogeneous surfaces and are mostly well characterized. The surface of glass exhibits already silanol groups intrinsically and consequentially demands only a removal of impurities. PDMS and Si_3N_4 however have different compositions as shown in Fig. 6 and ?? hence requiring a strong oxidation agents to completely exchange its interface to hydroxyl.[44–46]

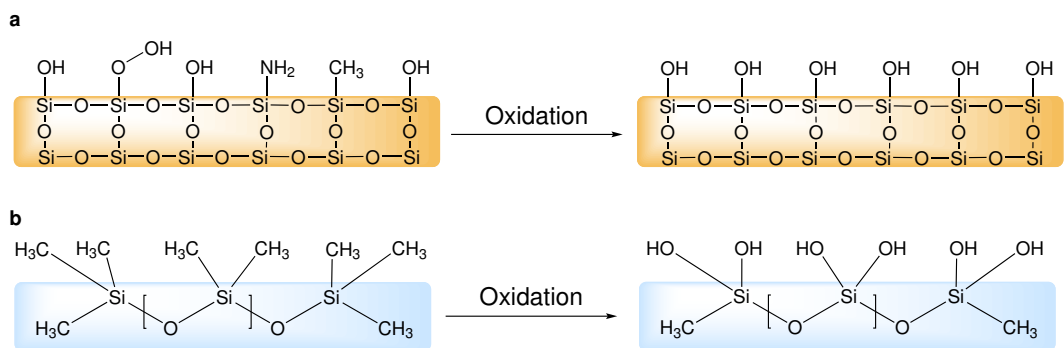
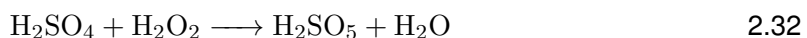


Figure 6: Different Substrate Surfaces: Glass, PDMS and Si_3N_4

Surface groups and internal structure of quartz glass (a), PDMS (b), and silicon nitride (c). After an oxidation step, the methyl groups are converted to hydroxyl.

Piranha Solution

Piranha is an oxidizer composed of hydrogen peroxide (H_2O_2) and H_2SO_4 , typically in volume ratios between 1:3 and 1:7. The effectiveness of piranha in removing organic residues and creating hydroxyl groups is induced by two distinct processes. First, hydrogen and oxygen are removed as units of water by the concentrated H_2SO_4 in a comparably fast process.(Eq. 2.32) This occurs due to the thermodynamically favorable reaction with an enthalpy of -880 kJ mol^{-1} and produces Caro's acid (H_2SO_5), one of the strongest oxidants known.[47]



Second, the sulfuric acid boosts hydrogen peroxide from a mild oxidizer into the more aggressive atomic oxygen by the dehydration of H_2O_2 . (Eq. 2.33) These two dehydration processes result on the one hand in a highly corrosive nature against organic

materials, particularly against the difficult to remove carbon. On the other hand, it is strongly acidic and oxidizing.

Hydrofluoric Acid

One of the substrates used in this work is Si_3N_4 as passivation layer above magnetic sensors as it has a significant better diffusion barrier against water or sodium ions and is chemically inert.[48] However, due to its complex crystal structure it is also difficult to modify by common chemicals and the exact surface composition still subject to scientific discussion.[49] Apart from cleaning the surface with piranha, few other modification methods have been reported, but only one suitable for the direct generation of hydroxyl groups.[42, 49–51]

As depicted in Fig. 6, the reaction $\text{Si}-\text{OH} + \text{HF} \leftrightarrow \text{Si}-\text{F} + \text{H}_2\text{O}$ takes place reversibly due to the coincidence that $\text{Si}-\text{O}$ and $\text{O}-\text{H}$ as well as $\text{Si}-\text{F}$ and $\text{H}-\text{F}$ bonds have similar binding energies. Hence, the forward and reverse reactions require a low activation energy. After Le Chatelier's principle, a depletion of HF in the bulk leads then to an increase in surficial hydroxyl groups.[52] It was revealed that an oxidation with a similar protocol based on aqueous HF yields a variable $\text{Si}-\text{O}-\text{Si}$ (siloxane) coverage with $37 \pm 17\%$ of a monolayer, which can be used for stable, covalent attachment of silanes. Nominally, the same surface coverages of silicon oxide and nitride surfaces could be achieved by ethoxy- and chlorosilanization.[53] As shown by Gustavsson et al. [54], the subsequent surfaces exhibit beneficial biological properties and can be modified by further standard procedures.

Oxygen Plasma

Apart from wet chemistry methods, the exposure of a surface to oxygen plasma yields hydroxyl groups as well. In a plasma chamber, a low-pressure gas is irradiated by kHz to MHz waves to excite and ionize its atoms. In consequence, the UV-radiation emitted by the gas can photolyse typical organic bonds and remove surface contaminations. Additionally, reactive oxygen species such as O_2^+ , O_2^- , O_3 or O oxidize the surface or bind dissociated components with low vapor pressure. During an evacuation in the process, these molecules are removed from the chamber intrinsically.[55]

1.2.2. Silane Chemistry

By the use of silane chemistry a surface is rendered organofunctional with alkoxy silane molecules. Since glass, silicon, alumina, titania, and quartz surfaces, as well as other metal oxide interfaces, are rich in hydroxyl groups, silanes are particularly useful for modifying these materials.[56]

The general formula for a silane coupling agent (Fig. 7a) typically shows the two classes of functionality. X is a hydrolyzable group typically alkoxy, acyloxy, halogen or amine. Following hydrolysis, a reactive silanol group is formed, which can condense with other silanol groups to form siloxane linkages. (Fig. 7) Stable condensation products are also formed with other oxides such as those of aluminum, zirconium, tin, titanium, and nickel. Less stable bonds are formed with oxides of boron, iron, and carbon, whereas alkali metal oxides and carbonates do not form stable bonds with siloxanes at all. The R group (Fig. 7a) is a nonhydrolyzable organic radical that may possess a functionality that imparts desired characteristics. One of the more common silanes is (3-aminopropyl)-triethoxysilane (APTES), where the X group consists of an $-O-CH_2-CH_3$ (ethoxy) group, the organic rest R is substituted by an $-NH_2$ (amine) and the 3 $-CH_2-$ (methylene) groups alter n to 3.[57]

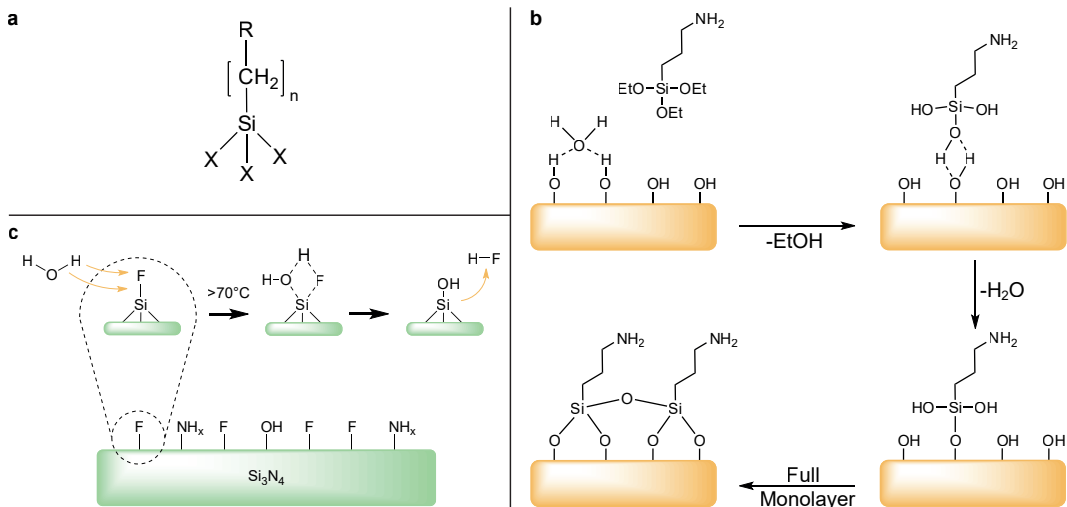


Figure 7: Surface Oxidation and Modification by APTES

(a) Structure of a typical trialkoxysilane, X: hydrolyzable group, R: non-hydrolyzable organic radical, n: methylene chain-length. (b) Before the condensation reaction, the oxidized surface has formed hydrogen bonds with water molecules while the silane molecules are in the bulk solution. The hydrolyzed silanol group adsorbs onto the surface and forms hydrogen bridges with the silicon bound oxygen atom. In a condensation reaction, under the loss of water, a covalent bond to the surface forms. After the SAM assembly the surface is saturated with a covalent-bound, crosslinked silane film.[58] (c) Proposed oxidation of Si_3N_4 with HF: Due to similar activation energies water can displace HF in a competitive manner effectively above a temperature above 70 °C.

The final result of reacting an organosilane with a substrate ranges from altering the

adhesion characteristics, catalyzing chemical transformation at the heterogeneous interface, ordering the interfacial region, and modifying its partition characteristics. Significantly, it includes the ability to effect a covalent bond between organic and inorganic materials. Especially in optical or biological sensors, silane modifications open a broad range of applications.[42, 59, 60]

However, the silanization reactions bear a few drawbacks which are often neglected. For instance, silane chemistry is strongly temperature and pH-dependent.[61, 62] Further, in a process to build SAMs from APTES, the reaction must be catalyzed by water. But already small changes in the water content cause dramatic deviations in layer thickness.[63] Additionally, silanes can crosslink to themselves through side reactions. (Fig. 7b) [64]

1.2.3. Carbodiimide Crosslinker Chemistry

By APTES amine-terminated films form the basis of many reactions and open the possibility to various applications, such as the direct attachment of biofunctional molecules by carbodiimide crosslinking chemistry.[65] Here, –COOH (carboxyl) groups are modified by 1-ethyl-3-(3-dimethylaminopropyl)carbodiimide (EDC) and N-hydroxysuccinimide (NHS) to form a stable secondary R₁–CONH–R₂ (carboxamide) bond with any primary amine.

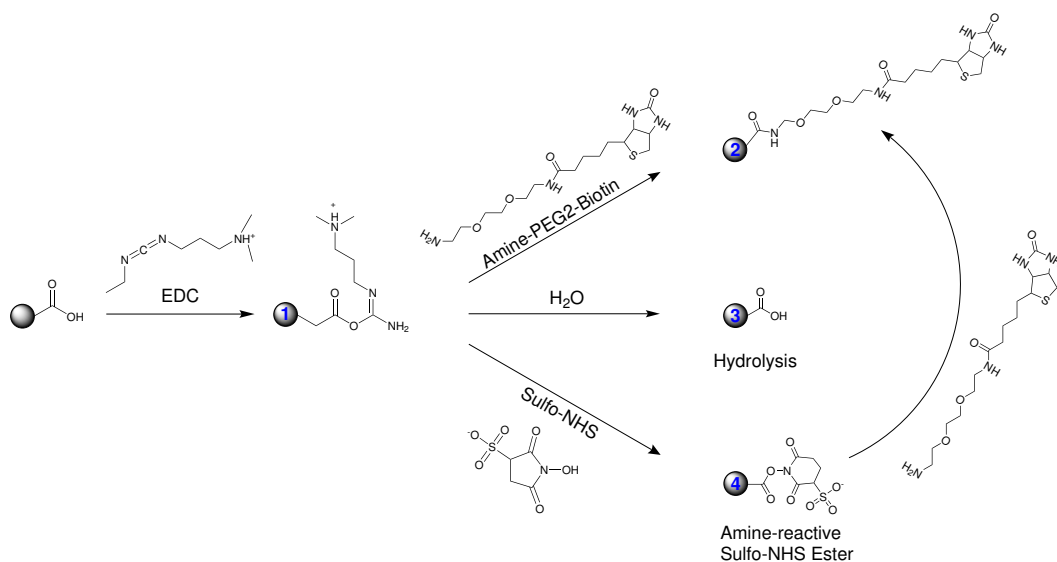


Figure 8: Carboxyl bead modification with EDC/NHS

The carboxyl groups on the bead are activated with EDC to an active O-acylisourea intermediate. This can then either be nucleophilically attacked by a primary amine of the amine-PEG₂-biotin reactant or - due to its instability - hydrolyzed back to a regenerated carboxyl surface. A present NHS-ester can also displace the O-acylisourea to form a considerably more stable intermediate which then itself reacts with any primary amine.

The general reaction mechanism is depicted in Fig. 8 for the example of a particle surface, but it can equivalently be applied to any other modified surface or molecule. The initial carboxyl group is esterified by EDC to an active o-acylisourea intermediate and leaves rapidly upon nucleophilic attack of an amine with release of an iso-urea byproduct. A zero-length amide linkage is formed. (Fig. 8, 1->2) Sulphydryl and hydroxyl groups also will react with such active esters, but the products of such reactions, thioesters and esters, are relatively unstable compared to an carboxamide bond. (Fig. 8, 1)[65]

However, this reactive complex is slow to react with amines and can hydrolyze in aqueous solutions. If the target amine does not find the active carboxyl before it hydrolyzes (Fig. 8, 3), the desired coupling cannot occur. This is especially a problem when the target molecule is in low concentration compared to water, as in the case of protein molecules. Notwithstanding, forming a NHS ester intermediate from the reaction of the hydroxyl group on NHS with the EDC active-ester complex increases the resultant amide bond formation remarkably. (Fig. 8, 4->2) [66]

Another critical point in carbodiimide chemistry is the solubility of the compounds. EDC, NHS and N-hydroxysulfosuccinimide (sulfo-NHS) are soluble in aqueous and organic solvents. Nevertheless, activation with non-sulfonate NHS decreases water-solubility of the modified carboxylate molecule, while activation with sulfo-NHS preserves or increases its water-solubility by virtue of the charged sulfonate group.[67]

1.2.4. The Biotin-Avidin-System

Until now, the interaction of the homotetrameric protein avidin and its ligand biotin forms one of the strongest known non-covalent bonds in biological systems characterized by a K_d in the range of 10^{-15} M.[68] First isolated from chicken egg white, it became a standard to use in biotechnology when researchers found a similar bacteria protein - streptavidin - in *Streptomyces* strains.[69] However, the charged glycoprotein avidin exhibits unspecific binding in some assays in comparison to streptavidin. Therefor, several companies developed deglycosylated forms of avidin with a neutral isoelectric points to minimize unspecificity. (NeutrAvidin, Extravidin, NeutraLite) In recent studies, a mutant streptavidin called "Traptavidin" exhibited an even 10 times dissociation rate.[70] As discovered in the early 1990s, biotin is bound inside a highly stable β -barrel structure, and stabilized by hydrogen bonds and van der Waals forces.[71] In a unique mechanism, a side group of biotin (valerate) binds to a neighboring monomer of streptavidin and therefor stabilizes the dimer complex intrinsically.[72, 73] From a thermodynamical point-of-view, the interaction of the vitamin and protein is described by a total free binding energy of 300 kJ mol^{-1} to 330 kJ mol^{-1} for a tetrameric protein.[73] All these aspects lead to a significant rupture force for the biotin-release of 250 pN .[74]

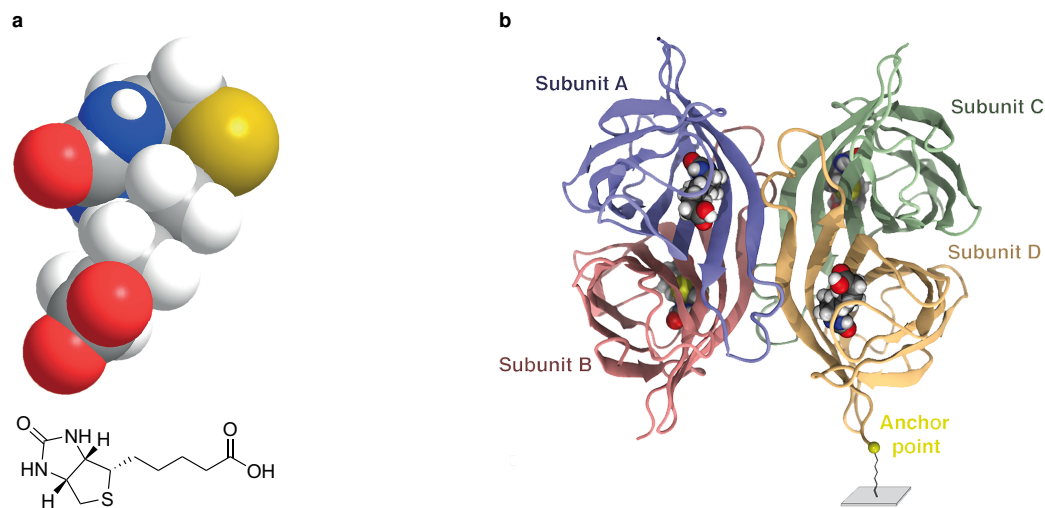


Figure 9: Functional Structures of Biotin and Streptavidin

(a) Two- and three dimensional chemical structure of the biotin molecule. (b) Homotetrameric streptavidin with four subunits and four bound biotin-ligands. The molecule is attached with the anchor point at one terminus to a surface.[75]

1.3. Magnetoresistive Sensing

The measurement system's main component is a GMR-sensor stack with a measured magnetoresistive effect of ~8 %. GMR is a quantum mechanical magnetoresistance effect observed in multilayers composed of alternating ferromagnetic and non-magnetic conductive layers. The driving factor for this resistance is anisotropy of a soft ferromagnetic layer. Two ferromagnetic layers with a thin conducting, non-magnetic spacer in the center build the base of the GMR stack.[76] One ferromagnetic layer has a so called pinned magnetization by exchange coupling, which is insensitive to outer magnetic fields. The second, "easy" layer is soft magnetic. Hence, it modulates its orientation in dependence to small coercive forces. [77]

In the case if both layers are aligned parallel, applying a current to the sensor allows majority charge carriers to pass through the layers with less impact into electrons on either sides. Accordingly, the overall resistance is low compared to another extremum in the antiparallel alignment. The magnetization direction can be controlled, for example, by applying an external magnetic field.[78, 79]

In the present system, GMR stacks were used in a Wheatstone configuration, where two bridges act as a reference for bridge balancing. In front of the sensor, nickel-based chevron patterns act as pre-enrichment for magnetic particles. These structures are driven by an external permanent magnet hence imposing a high flux density gradient on particles. Above these patterns, previously mentioned Si_3N_4 passivation has been deposited in various thicknesses to achieve inertness. On top of the sensor chip, a straight microfluidic channel is mounted to execute flow cytometry experiments.[80, 81]

In order to measure the change in resistance sensitively, the lock-in principle is used.

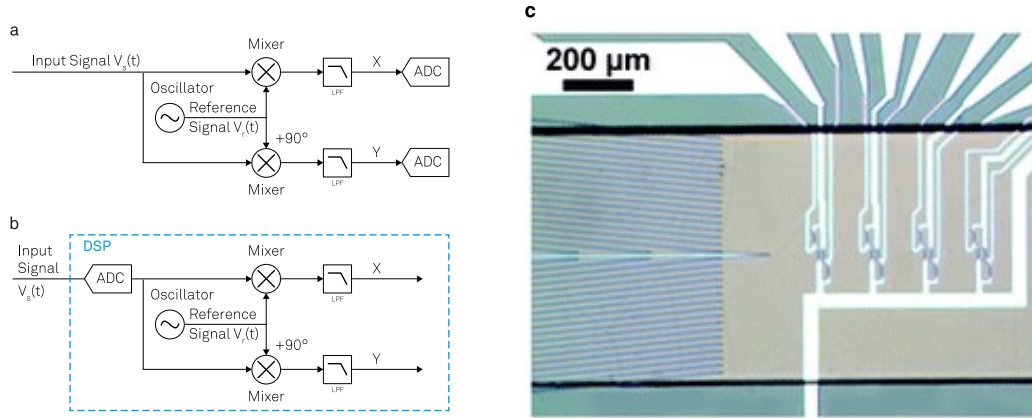


Figure 10: MRCyte Overview
Nice image of the MRCyte system with microscope.

Here, an amplifier extracts signals in a defined frequency band around a reference frequency. This efficiently filters all other frequency components. Thereby a lock-in amplifier performs a multiplication of its input $V_s(t)$ with a reference signal $V_r(t)$ and low-pass filters the result $Z(t)$. In most integrated cases, the reference signal is generated additionally by the lock-in amplifier itself. Using a pure sine wave as reference enables a selective measurement at the fundamental frequency or its harmonics.[82] At a measurement, $V_s(t)$ is split and separately multiplied with the reference signal and a 90° phase-shifted copy of it. After demodulation, the result is constituted from signal components at the sum and the difference of signal and the reference frequency, ω_s and ω_r , respectively.(Eqs. 3.34 to 3.36) In the resulting signal, the trigonometric functions are Euler transformed and the magnitude $R = \sqrt{X(t)^2 + Y(t)^2}$ acts as measurand. The high frequency compounds are then filtered digitally by a low-pass filter of varying order n to increase signal-to-noise ratio (SNR). As described in Eq. 3.38, a low-pass in the frequency domain can be described by a power series of first-order filters.

$$V_s(t) = \sqrt{2}R \cdot \cos(\omega_s t + \Theta) \quad 3.34$$

$$V_r(t) = \sqrt{2}e^{-i\omega_r t} = \sqrt{2} \cos(\omega_r t) - i\sqrt{2} \sin(\omega_r t) \quad 3.35$$

$$Z(t) = X(t) + iY(t) = V_s(t) \cdot V_r(t) \quad 3.36$$

$$= R \left[e^{i((\omega_z - \omega_r)t + \theta)} + e^{-i[(\omega_z + \omega_r)t + \theta]} \right] \quad 3.37$$

$$H_n(\omega) = H_1(\omega)^n = \left(\frac{1}{1 + i\omega\tau} \right)^n \quad 3.38$$

However, with this measurement principle SNR can not increase infinitely. If the signal strength cannot be increased, the noise has to be reduced or avoided as much as possible. Nevertheless, noise is always caused by different sources in analog signals, for example thermal, shot, and flicker noise. Other sources are of technical origin, as for example ground loops, crosstalk, 50 Hz noise or electromagnetic pick-up. [82]

Now, to characterize a GMR with the lock-in, the easy layer has to be deflected to the full extents. For this, Helmholtz coils impose a high field in the orthogonal direction. The lock-in captures a hysteresis during the sweep from parallel to anti-parallel alignment of the layers at a specific bridge circuit. The steepness hereby indicates the sensitivity of the sensor element in the units V T^{-1} .

List of Abbreviations

Symbols

Q - flow rate.....
χ - magnetic susceptibility
η - dynamic viscosity.....
μF - microfluidic
ω - angular rotation frequency
τ - surface stress tensor.....
$\tau_{pressure}$ - pressure stress tensor.....
$\tau_{viscous}$ - viscous stress tensor
ε - shear stress tensor
B - magnetic flux density.....
$F_{buoyancy}$ - buoyancy.....
F_{drag} - Stoke's drag force
F_{el} - Coulomb's force.....
F_{grav} - gravity
F_{magnus} - Magnus lift force
F_{mag} - magentic force
$F_{saffman}$ - Saffman lift force.....
F_{shear} - shear-induced lift force
M - magnetization.....
T_{crit} - critical tension.....
Ω - rotation vector
m - magnetic dipole moment
u - flow field.....
u_s - sedimentation velocity.....
Re - Reynolds number
$Re_{particle}$ - particle Reynolds number.....
\vec{n} - unit outward normal
ρ - density
$\sum_i F_i$ - body forces

A

AAF - artificial Anti-Ferromagnet.....
AcOH - acetic acid.....
AFM - Anti-Ferromagnetism.....
amine - –NH ₂
APTES - (3-aminopropyl)triethoxysilane

C

carboxamide - R ₁ – CONH – R ₂
carboxyl - –COOH
CV - coefficient of variance

D

diH ₂ O - deionized water
DMSO - dimethyl sulfoxide.....

E

EDC - 1-ethyl-3-(3-dimethylaminopropyl)carbodiimide
ethoxy - –O –CH ₂ – CH ₃
EtOH - ethanol

F

FM - Ferrimagnetism.....
FWHM - full width at half maximum.....

G

GMR - giant magneto resistance

H

H ₂ O ₂ - hydrogen peroxide
H ₂ SO ₅ - Caro's acid.....
H ₂ SO ₄ - sulfuric acid.....
HCl - hydrochloric acid
HF - hydrofluoric acid.....
hydroxyl - –OH

I

I
IPA - isopropanol.....

K

K_d - dissociation constant.....

M

MACS - MACS running buffer.....

MeOH - methanol.....

MES - 2-(N-morpholino)ethanesulfonic acid.....

MEST - 2-(N-morpholino)ethanesulfonic acid (MES) buffer with Tween 20

methylene - –CH₂ –

MFI - median fluorescence intensity.....

MFLI - multi frequency lock-in

MNP - magnetic nanoparticle.....

N

N₂ - nitrogen gas.....

NFM - non-ferro-magnetic.....

NHS - N-hydroxysuccinimide.....

NSE - Navier-Stokes-Equation

O

O₂ - oxygen gas.....

P

PAA - Poly(acrylic) Acid.....

PBS - phosphate buffered saline

PBST - phosphate buffered saline (PBS) with Tween 20

PCB - printed circuit board.....

PDMS - poly(dimethyl siloxane).....

piranha - a mixture from hydrogen peroxide with excess of sulfuric acid.....

PM - Paramagnetism

R

RBC - red blood cell.....

S

SAM - self-assembled monolayer
Si_3N_4 - silicon nitride
silanol - Si–OH
siloxane - Si–O–Si
SMA - styrene maleic anhydride
SNR - signal-to-noise ratio
SPM - superparamagnetism
sulfo-NHS - N-hydroxysulfosuccinimide

V

V_{pp} - peak-to-peak voltage
V_p - peak voltage

Z

z - approach

List of Figures

1 Particle Drag and Lift Behavior	
(a) Bulk Drag: Force acts on a particle caused by the displacement of fluid stream lines. (b) Wall-lift Drag Force: In a special case of drag, where streamlines cannot be displaced further, a pressure gradient forms in front of the sphere. This forces a motion directed perpendicularly from the wall. (c) Shear-induced force: The curvature of the flow profile exhibits a translation and rotation due to inhomogeneously distributed shear on the surface.[11]	5
2 Particle Rotation Behavior	
(a) Direction of rotation of a sphere settling in eccentric position between parallel walls. (b) Direction of rotation of a sphere settling in the presence of a single plane wall far from the other side.[10]	6
3 Magnus Effect on a Particle in Laminar Flow	
The intrinsic rotation of a particle inside a laminar flow field causes a pressure gradient to the side whose tangential rotation vector is parallel to the stream lines.	8
4 Rolling Mechanics of a Sphere	
Penetration model of a sphere with radius r adapted from Azad and Featherstone [25] and Waters and Guduru [26]. The top body moves into the elastic bottom body for an approach (z) and a contact area πa^2	11
5 Membrane Adhesion and Detachment Models	
a Adhesion Model after Dembo et al. [29]: Every interaction is viewed as spring-damper-model in superposition. b Surface Coverage Assay Model: In a stochastic approach, analyte molecules and their interactions are modeled between a planar and a spherical surface. Adapted from Wu and Voldman [9]	13

6	Different Substrate Surfaces: Glass, PDMS and Si₃N₄	
	Surface groups and internal structure of quartz glass (a), PDMS (b), and silicon nitride (c). After an oxidation step, the methyl groups are converted to hydroxyl.	16
7	Surface Oxidation and Modification by APTES	
	(a) Structure of a typical trialkoxysilane, X: hydrolyzable group, R: non-hydrolyzable organic radical, n: methylene chain-length. (b) Before the condensation reaction, the oxidized surface has formed hydrogen bonds with water molecules while the silane molecules are in the bulk solution. The hydrolyzed silanol group adsorbs onto the surface and forms hydrogen bridges with the silicon bound oxygen atom. In a condensation reaction, under the loss of water, a covalent bond to the surface forms. After the SAM assembly the surface is saturated with a covalent-bound, crosslinked silane film.[58] (c) Proposed oxidation of Si ₃ N ₄ with HF: Due to similar activation energies water can displace HF in a competitive manner effectively above a temperature above 70 °C.	18
8	Carboxyl bead modification with EDC/NHS	
	The carboxy groups bead are activated with EDC to an active O-acylisourea intermediate. This can then either be nucleophilicly attacked by a primary amine of the amine-PEG ₂ -biotin reactant or - due to its instability - hydrolyzed back to a regenerated carboxyl surface. A present NHS-ester can also displace the O-acylisourea to form a considerably more stable intermediate which then itself reacts with any primary amine.	19
9	Functional Structures of Biotin and Streptavidin	
	(a) Two- and three dimensional chemical structure of the biotin molecule. (b) Homotetrameric streptavidin with four subunits and four bound biotin-ligands. The molecule is attached with the anchor point at one terminus to a surface.[75]	21
10	MRCyte Overview	
	Nice image of the MRCyte system with microscope.	22

List of Tables

Bibliography

- [1] Michael Helou. "Magnetic Flow Cytometry". PhD Thesis. 2014.
- [2] Mathias Reisbeck. "Integration und quantitative Analyse in der magnetischen Durchflusszytometrie". Thesis. 2019.
- [3] Johann Brenner. "Superparamagnetic Nanoparticles in Picoliter Droplets for Measurements with Spin Valves". Bachelor Thesis. 2018.
- [4] Esther Räth. "Affinity-based Cell Rolling Assays in Magnetic Flow Cytometry". Thesis. 2020.
- [5] Brian Kirby. *Micro- and Nanoscale Fluid Mechanics*. 2010. ISBN: 9780511760723. DOI: 10.1017/cbo9780511760723.
- [6] Henrik Bruus. *Theoretical Microfluidics*. Technical University of Denmark: Oxford University Press, 2008. ISBN: 978–0–19–923508–7.
- [7] Hyungoo Lee and S. Balachandar. "Drag and lift forces on a spherical particle moving on a wall in a shear flow at finite Re ". In: *Journal of Fluid Mechanics* 657 (2010), pp. 89–125. ISSN: 0022-1120. DOI: 10.1017/s0022112010001382.
- [8] Cheng Dong and Xiao X. Lei. "Biomechanics of cell rolling: shear flow, cell-surface adhesion, and cell deformability". In: *Journal of Biomechanics* 33.1 (2000), pp. 35–43. ISSN: 00219290. DOI: 10.1016/s0021-9290(99)00174-8.
- [9] Dan Wu and Joel Voldman. "An integrated model for bead-based immunoassays". In: *Biosensors and Bioelectronics* 154 (2020). ISSN: 09565663. DOI: 10.1016/j.bios.2020.112070.
- [10] D. Di Carlo et al. "Continuous inertial focusing, ordering, and separation of particles in microchannels". In: *Proceedings of the National Academy of Sciences* 104.48 (2007), pp. 18892–18897. ISSN: 0027-8424. DOI: 10.1073/pnas.0704958104.
- [11] Joseph M. Martel and Mehmet Toner. "Inertial Focusing in Microfluidics". In: *Annual Review of Biomedical Engineering* 16.1 (2014). PMID: 24905880, pp. 371–396. DOI: 10.1146/annurev-bioeng-121813-120704.
- [12] Howard Brenner. "The slow motion of a sphere through a viscous fluid towards a plane surface". In: *Chemical Engineering Science* 16.3-4 (Dec. 1961), pp. 242–251. DOI: 10.1016/0009-2509(61)80035-3.

- [13] John Happel and Howard Brenner. *Low Reynolds number hydrodynamics*. Mechanics of fluids and transport processes. 1981. ISBN: 978-94-009-8352-6. DOI: 10.1007/978-94-009-8352-6.
- [14] Lanying Zeng et al. “Forces on a finite-sized particle located close to a wall in a linear shear flow”. In: *Physics of Fluids* 21.3 (2009), p. 033302. ISSN: 1070-6631. DOI: 10.1063/1.3082232.
- [15] Rune Barnkob et al. “Acoustic radiation- and streaming-induced microparticle velocities determined by microparticle image velocimetry in an ultrasound symmetry plane”. In: *Physical Review E* 86.5 (2012). ISSN: 1539-3755. DOI: 10.1103/physreve.86.056307.
- [16] Jun Zhang et al. “Fundamentals and applications of inertial microfluidics: a review”. In: *Lab on a Chip* 16.1 (2016), pp. 10–34. ISSN: 1473-0197. DOI: 10.1039/c5lc01159k.
- [17] Ewa Guzniczak et al. “Deformability-induced lift force in spiral microchannels for cell separation”. In: *Lab on a Chip* 20.3 (2020), pp. 614–625. ISSN: 1473-0197. DOI: 10.1039/c9lc01000a.
- [18] Albert J. Mach and Dino Di Carlo. “Continuous scalable blood filtration device using inertial microfluidics”. In: *Biotechnology and Bioengineering* 107.2 (June 2010), pp. 302–311. DOI: 10.1002/bit.22833.
- [19] Robin Fåhræus and Torsten Lindqvist. “THE VISCOSITY OF THE BLOOD IN NARROW CAPILLARY TUBES”. In: *American Journal of Physiology-Legacy Content* 96.3 (Mar. 1931), pp. 562–568. DOI: 10.1152/ajplegacy.1931.96.3.562.
- [20] Robin Fåhræus. “THE SUSPENSION STABILITY OF THE BLOOD”. In: *Physiological Reviews* 9.2 (Apr. 1929), pp. 241–274. DOI: 10.1152/physrev.1929.9.2.241.
- [21] G. Segré and A. Silberberg. “Radial Particle Displacements in Poiseuille Flow of Suspensions”. In: *Nature* 189.4760 (Jan. 1961), pp. 209–210. DOI: 10.1038/189209a0.
- [22] Rachid Chebbi. “Dynamics of blood flow: modeling of the Fåhræus–Lindqvist effect”. In: *Journal of Biological Physics* 41.3 (Feb. 2015), pp. 313–326. DOI: 10.1007/s10867-015-9376-1.
- [23] Koffi Espoir Koumi, Thibaut Chaise, and Daniel Nelias. “Rolling contact of a rigid sphere/sliding of a spherical indenter upon a viscoelastic half-space containing

- an ellipsoidal inhomogeneity". In: *Journal of the Mechanics and Physics of Solids* 80 (July 2015), pp. 1–25. DOI: 10.1016/j.jmps.2015.04.001.
- [24] Bo Jacobson and Joost J. Kalker, eds. *Rolling Contact Phenomena*. Springer Vienna, 2000. DOI: 10.1007/978-3-7091-2782-7.
- [25] M. Azad and R. Featherstone. "Modeling the contact between a rolling sphere and a compliant ground plane". In: 2010.
- [26] Julie F. Waters and Pradeep R. Guduru. "Mode-mixity-dependent adhesive contact of a sphere on a plane surface". In: *Proceedings of the Royal Society A: Mathematical, Physical and Engineering Sciences* 466.2117 (Dec. 2009), pp. 1303–1325. DOI: 10.1098/rspa.2009.0461.
- [27] Gokul P. Krishnan and David T. Leighton. "Inertial lift on a moving sphere in contact with a plane wall in a shear flow". In: *Physics of Fluids* 7.11 (1995), pp. 2538–2545. ISSN: 1070-6631. DOI: 10.1063/1.868755.
- [28] R. P. McEver and C. Zhu. "Rolling cell adhesion". In: *Annu Rev Cell Dev Biol* 26 (2010), pp. 363–96. ISSN: 1530-8995 (Electronic) 1081-0706 (Linking). DOI: 10.1146/annurev.cellbio.042308.113238.
- [29] M. Dembo et al. "The reaction-limited kinetics of membrane-to-surface adhesion and detachment". In: *Proceedings of the Royal Society of London. Series B. Biological Sciences* 234.1274 (1997), pp. 55–83. ISSN: 0080-4649 2053-9193. DOI: 10.1098/rspb.1988.0038.
- [30] Pavel I. Kitov and David R. Bundle. "On the Nature of the Multivalency Effect: A Thermodynamic Model". In: *Journal of the American Chemical Society* 125.52 (2003), pp. 16271–16284. ISSN: 0002-7863. DOI: 10.1021/ja038223n.
- [31] Bryan T. Marshall et al. "Direct observation of catch bonds involving cell-adhesion molecules". In: *Nature* 423.6936 (2003), pp. 190–193. ISSN: 0028-0836. DOI: 10.1038/nature01605.
- [32] Krishna K. Sarangapani et al. "Low Force Decelerates L-selectin Dissociation from P-selectin Glycoprotein Ligand-1 and Endoglycan*". In: *Journal of Biological Chemistry* 279.3 (2004), pp. 2291–2298. ISSN: 0021-9258. DOI: <https://doi.org/10.1074/jbc.M310396200>.
- [33] H. Cumhur Tekin, Matteo Cornaglia, and Martin A. M. Gijs. "Attomolar protein detection using a magnetic bead surface coverage assay". In: *Lab on a Chip* 13.6 (2013), p. 1053. ISSN: 1473-0197. DOI: 10.1039/c3lc41285g.

- [34] S. Prentner et al. "Effects of channel surface finish on blood flow in microfluidic devices". In: *Microsystem Technologies* 16.7 (2010), pp. 1091–1096. ISSN: 0946-7076. DOI: 10.1007/s00542-009-1004-1.
- [35] Li-Chong Xu, James W. Bauer, and Christopher A. Siedlecki. "Proteins, platelets, and blood coagulation at biomaterial interfaces". In: *Colloids and Surfaces B: Biointerfaces* 124 (2014), pp. 49–68. ISSN: 0927-7765. DOI: 10.1016/j.colsurfb.2014.09.040.
- [36] Sushanta K. Mitra and Auro Ashish Saha. "Surface Modification, Methods". In: *Encyclopedia of Microfluidics and Nanofluidics*. Springer US, 2014, pp. 1–9. DOI: 10.1007/978-3-642-27758-0_1503-2.
- [37] R.A. Williams and H.W. Blanch. "Covalent immobilization of protein monolayers for biosensor applications". In: *Biosensors and Bioelectronics* 9.2 (1994), pp. 159–167. ISSN: 0956-5663. DOI: 10.1016/0956-5663(94)80108-8.
- [38] William Putzbach and Niina Ronkainen. "Immobilization Techniques in the Fabrication of Nanomaterial-Based Electrochemical Biosensors: A Review". In: *Sensors* 13.4 (2013), pp. 4811–4840. ISSN: 1424-8220. DOI: 10.3390/s130404811.
- [39] R. Funari et al. "Single Molecule Characterization of UV-Activated Antibodies on Gold by Atomic Force Microscopy". In: *Langmuir* 32.32 (2016), pp. 8084–8091. ISSN: 0743-7463. DOI: 10.1021/acs.langmuir.6b02218.
- [40] A. Ymeti et al. "Integration of microfluidics with a four-channel integrated optical Young interferometer immunosensor". In: *Biosensors and Bioelectronics* 20.7 (2005), pp. 1417–1421. ISSN: 0956-5663. DOI: <https://doi.org/10.1016/j.bios.2004.04.015>.
- [41] María-José Bañuls, Rosa Puchades, and Ángel Maquieira. "Chemical surface modifications for the development of silicon-based label-free integrated optical (IO) biosensors: A review". In: *Analytica Chimica Acta* 777 (2013), pp. 1–16. ISSN: 0003-2670. DOI: 10.1016/j.aca.2013.01.025.
- [42] N. Lange. "Selective Chemical Modification of Silicon Nitride Surfaces for Novel Biosensor Application". Thesis. 2017. DOI: <http://dx.doi.org/10.17169/refubium-11275>.
- [43] Marine Brunet et al. "Etching and Chemical Control of the Silicon Nitride Surface". In: *ACS Applied Materials & Interfaces* 9.3 (2017), pp. 3075–3084. ISSN: 1944-8244. DOI: 10.1021/acsami.6b12880.

- [44] K. Sekine et al. "Highly robust ultrathin silicon nitride films grown at low-temperature by microwave-excitation high-density plasma for giga scale integration". In: *IEEE Transactions on Electron Devices* 47.7 (2000), pp. 1370–1374. ISSN: 0018-9383. DOI: 10.1109/16.848279.
- [45] M. K. Chaudhury and G. M. Whitesides. "Correlation Between Surface Free Energy and Surface Constitution". In: *Science* 255.5049 (1992), pp. 1230–1232. ISSN: 0036-8075. DOI: 10.1126/science.255.5049.1230.
- [46] H. Hillborg et al. "Crosslinked polydimethylsiloxane exposed to oxygen plasma studied by neutron reflectometry and other surface specific techniques". In: *Polymer* 41.18 (2000), pp. 6851–6863. ISSN: 0032-3861. DOI: [https://doi.org/10.1016/S0032-3861\(00\)00039-2](https://doi.org/10.1016/S0032-3861(00)00039-2).
- [47] A. N. Ermakov et al. "The thermodynamic characteristics of hydrogen peroxide in H₂SO₄-H₂O solutions". In: *Russian Journal of Physical Chemistry A* 80.12 (2006), pp. 1895–1901. ISSN: 0036-0244. DOI: 10.1134/s0036024406120041.
- [48] Masatomo Yashima, Yoshiaki Ando, and Yasunori Tabira. "Crystal Structure and Electron Density of α -Silicon Nitride: Experimental and Theoretical Evidence for the Covalent Bonding and Charge Transfer". In: *The Journal of Physical Chemistry B* 111.14 (2007), pp. 3609–3613. ISSN: 1520-6106. DOI: 10.1021/jp0678507.
- [49] Marine Brunet et al. "Etching and Chemical Control of the Silicon Nitride Surface". In: *ACS Applied Materials & Interfaces* 9.3 (2017), pp. 3075–3084. ISSN: 1944-8244. DOI: 10.1021/acsami.6b12880.
- [50] Ahmed Arafat et al. "Covalent Biofunctionalization of Silicon Nitride Surfaces". In: *Langmuir* 23.11 (2007), pp. 6233–6244. ISSN: 0743-7463 1520-5827. DOI: 10.1021/la7007045.
- [51] Michel Rosso. *Modification of Silicon Nitride and Silicon Carbide Surfaces for Food and Biosensor Applications*. 2009. ISBN: 978-90-8585-379-4.
- [52] David J. Michalak et al. "Nanopatterning Si(111) surfaces as a selective surface-chemistry route". In: *Nature Materials* 9.3 (2010), pp. 266–271. ISSN: 1476-1122. DOI: 10.1038/nmat2611.
- [53] L. H. Liu et al. "Surface etching, chemical modification and characterization of silicon nitride and silicon oxide—selective functionalization of Si₃N₄ and SiO₂". In: *J Phys Condens Matter* 28.9 (2016), p. 094014. ISSN: 1361-648X (Electronic) 0953-8984 (Linking). DOI: 10.1088/0953-8984/28/9/094014.

- [54] Johan Gustavsson et al. "Surface modifications of silicon nitride for cellular biosensor applications". In: *Journal of Materials Science: Materials in Medicine* 19.4 (2008), pp. 1839–1850. ISSN: 0957-4530. DOI: 10.1007/s10856-008-3384-7.
- [55] A. Pizzi and K.L. Mittal. *Handbook of Adhesive Technology, Revised and Expanded*. Taylor and Francis, 2003. ISBN: 9780203912225.
- [56] Brian Seed. "Silanizing Glassware". In: *Current Protocols in Cell Biology* 8.1 (2000), A.3E.1–A.3E.2. ISSN: 1934-2500. DOI: 10.1002/0471143030.cba03es08.
- [57] GELEST. *Silane Coupling Agents*. Catalog. 2014.
- [58] Hossein Khanjanzadeh et al. "Application of surface chemical functionalized cellulose nanocrystals to improve the performance of UF adhesives used in wood based composites - MDF type". In: *Carbohydrate Polymers* 206 (2019), pp. 11–20. ISSN: 0144-8617. DOI: <https://doi.org/10.1016/j.carbpol.2018.10.115>.
- [59] K. C. Andree et al. "Capture of Tumor Cells on Anti-EpCAM-Functionalized Poly(acrylic acid)-Coated Surfaces". In: *ACS Appl Mater Interfaces* 8.23 (2016), pp. 14349–56. ISSN: 1944-8252 (Electronic) 1944-8244 (Linking). DOI: 10.1021/acsami.6b01241.
- [60] Solange Magalhães et al. "Brief Overview on Bio-Based Adhesives and Sealants". In: *Polymers* 11.10 (2019), p. 1685. ISSN: 2073-4360. DOI: 10.3390/polym11101685.
- [61] Nina Bjørk Arnfinnsdottir et al. "Impact of Silanization Parameters and Antibody Immobilization Strategy on Binding Capacity of Photonic Ring Resonators". In: *Sensors* 20.11 (2020). ISSN: 1424-8220. DOI: 10.3390/s20113163.
- [62] Robert M. Pasternack, Sandrine Rivillon Amy, and Yves J. Chabal. "Attachment of 3-(Aminopropyl)triethoxysilane on Silicon Oxide Surfaces: Dependence on Solution Temperature". In: *Langmuir* 24.22 (2008), pp. 12963–12971. ISSN: 0743-7463. DOI: 10.1021/la8024827.
- [63] M. J. Banuls et al. "Selective chemical modification of silicon nitride/silicon oxide nanostructures to develop label-free biosensors". In: *Biosens Bioelectron* 25.6 (2010), pp. 1460–6. ISSN: 1873-4235 (Electronic) 0956-5663 (Linking). DOI: 10.1016/j.bios.2009.10.048.
- [64] Dean W. Sindorf and Gary E. Maciel. "Solid-state NMR studies of the reactions of silica surfaces with polyfunctional chloromethylsilanes and ethoxymethylsilanes". In: *Journal of the American Chemical Society* 105.12 (1983), pp. 3767–3776. ISSN: 0002-7863. DOI: 10.1021/ja00350a003.

- [65] *Bioconjugate Techniques*. Elsevier, 2013. DOI: 10.1016/c2009-0-64240-9.
- [66] D.G. Hoare and D.E. Koshland. “A Method for the Quantitative Modification and Estimation of Carboxylic Acid Groups in Proteins”. In: *Journal of Biological Chemistry* 242.10 (May 1967), pp. 2447–2453. DOI: 10 . 1016 / s0021 - 9258(18)95981-8.
- [67] ThermoFisher Scientific. *User Guide: NHS and Sulfo-NHS*. 2021.
- [68] D. W. Woolley and L. G. Longsworth. “Isolation of an antibiotic factor from egg white.” In: *Journal of Biological Chemistry* 142 (1942), pp. 285–290.
- [69] T. Sano and C. R. Cantor. “Expression of a cloned streptavidin gene in Escherichia coli.” In: *Proceedings of the National Academy of Sciences* 87.1 (1990), pp. 142–146. ISSN: 0027-8424. DOI: 10 . 1073/pnas . 87 . 1 . 142.
- [70] Claire E Chivers et al. “A streptavidin variant with slower biotin dissociation and increased mechanostability”. In: *Nature Methods* 7.5 (2010), pp. 391–393. ISSN: 1548-7091. DOI: 10 . 1038/nmeth . 1450.
- [71] P. Weber et al. “Structural origins of high-affinity biotin binding to streptavidin”. In: *Science* 243.4887 (1989), pp. 85–88. ISSN: 0036-8075. DOI: 10 . 1126/science . 2911722.
- [72] Bruno Miroux and John E. Walker. “Over-production of Proteins in Escherichia coli: Mutant Hosts that Allow Synthesis of some Membrane Proteins and Globular Proteins at High Levels”. In: *Journal of Molecular Biology* 260.3 (1996), pp. 289–298. ISSN: 0022-2836. DOI: 10 . 1006/jmbi . 1996 . 0399.
- [73] Shuichi Miyamoto and Peter A. Kollman. “Absolute and relative binding free energy calculations of the interaction of biotin and its analogs with streptavidin using molecular dynamics/free energy perturbation approaches”. In: *Proteins: Structure, Function, and Bioinformatics* 16.3 (1993), pp. 226–245. ISSN: 0887-3585. DOI: 10 . 1002/prot . 340160303.
- [74] H., B. Heymann, and P. Tavan. “Ligand Binding: Molecular Mechanics Calculation of the Streptavidin-Biotin Rupture Force”. In: *Science* 271.5251 (1996), pp. 997–999. ISSN: 0036-8075. DOI: 10 . 1126/science . 271 . 5251 . 997.
- [75] Steffen M. Sedlak et al. “Streptavidin/biotin: Tethering geometry defines unbinding mechanics”. In: *Science Advances* 6.13 (2020). DOI: 10 . 1126 / sciadv . aay5999.
- [76] Carmen-Gabriela Stefanita. *Magnetism*. Springer Berlin Heidelberg, 2012. DOI: 10 . 1007/978-3-642-22977-0.

- [77] Alberto P. Guimarães. *Principles of Nanomagnetism*. Springer International Publishing, 2017. DOI: 10.1007/978-3-319-59409-5.
- [78] K. H. J. Buschow and F. R. de Boer. *Physics of Magnetism and Magnetic Materials*. Springer US, 2003. DOI: 10.1007/b100503.
- [79] Hugo Dr. van den Berg. “Magnetoresistance sensor using multi-layer system - has intermediate layer between measuring layer and bias layer with perpendicular magnetisation”. DE4232244A1. May 14, 1998.
- [80] Michael Helou et al. “Time-of-flight magnetic flow cytometry in whole blood with integrated sample preparation”. In: *Lab on a Chip* 13.6 (2013), p. 1035. DOI: 10.1039/c3lc41310a.
- [81] Mathias Reisbeck et al. “Magnetic fingerprints of rolling cells for quantitative flow cytometry in whole blood”. In: *Scientific Reports* 6.1 (Sept. 2016). DOI: 10.1038/srep32838.
- [82] *Principles of lock-in detection and the state of the art*. 2016. URL: <https://www.zhinst.com/others/en/resources/principles-of-lock-in-detection>.
- [83] micromod Partikeltechnologie GmbH. *TECHNICAL DATA SHEET - nanomag®-D-spio 50nm*. 2018.
- [84] Michael J. Owen and Patrick J. Smith. “Plasma treatment of polydimethylsiloxane”. In: *Journal of Adhesion Science and Technology* 8.10 (1994), pp. 1063–1075. DOI: 10.1163/156856194X00942.
- [85] Georgia C. Papaefthymiou. “Nanoparticle magnetism”. In: *Nano Today* 4.5 (Oct. 2009), pp. 438–447. DOI: 10.1016/j.nantod.2009.08.006.
- [86] P Gravesen, J Branebjerg, and O S Jensen. “Microfluidics-a review”. In: *Journal of Micromechanics and Microengineering* 3.4 (Dec. 1993), pp. 168–182. DOI: 10.1088/0960-1317/3/4/002.
- [87] Walter J. Dressick et al. “Covalent Binding of Pd Catalysts to Ligating Self-Assembled Monolayer Films for Selective Electroless Metal Deposition”. In: *Journal of the Electrochemical Society* 141.1 (1994), pp. 210–220. ISSN: 0013-4651. DOI: 10.1149/1.2054686.
- [88] Rojda Hicsanmaz. “Setup and Assessment of Laser Lithography for the Fabrication and Integration of Biosensor and Microfluidic Devices”. Technical University Munich, 2020.

- [89] *Syringe pumps*. 2021. URL: <https://www.fluigent.com/resources/microfluidic-expertise/what-is-microfluidic/system-comparison-for-microfluidic-applications/>.
- [90] K. C. Andree et al. “Capture of Tumor Cells on Anti-EpCAM-Functionalized Poly(acrylic acid)-Coated Surfaces”. In: *ACS Appl Mater Interfaces* 8.23 (2016), pp. 14349–56. ISSN: 1944-8252 (Electronic) 1944-8244 (Linking). DOI: 10.1021/acsami.6b01241.
- [91] Giuseppe Antonacci et al. “Ultra-sensitive refractive index gas sensor with functionalized silicon nitride photonic circuits”. In: *APL Photonics* 5.8 (2020). ISSN: 2378-0967. DOI: 10.1063/5.0013577.
- [92] A. Arafat et al. “Tailor-made functionalization of silicon nitride surfaces”. In: *J Am Chem Soc* 126.28 (2004), pp. 8600–1. ISSN: 0002-7863 (Print) 0002-7863 (Linking). DOI: 10.1021/ja0483746.
- [93] B. Baur et al. “Chemical functionalization of GaN and AlN surfaces”. In: *Applied Physics Letters* 87.26 (2005), p. 263901. ISSN: 0003-6951. DOI: 10.1063/1.2150280.
- [94] J. Diao et al. “A surface modification strategy on silicon nitride for developing biosensors”. In: *Anal Biochem* 343.2 (2005), pp. 322–8. ISSN: 0003-2697 (Print) 0003-2697 (Linking). DOI: 10.1016/j.ab.2005.05.010.
- [95] T. Ghonge et al. “Smartphone-imaged microfluidic biochip for measuring CD64 expression from whole blood”. In: *Analyst* 144.13 (2019), pp. 3925–3935. ISSN: 1364-5528 (Electronic) 0003-2654 (Linking). DOI: 10.1039/c9an00532c.
- [96] Markus Hofstetter et al. “In vitro bio-functionality of gallium nitride sensors for radiation biophysics”. In: *Biochemical and Biophysical Research Communications* 424.2 (2012), pp. 348–353. ISSN: 0006-291X. DOI: 10.1016/j.bbrc.2012.06.142.
- [97] D. Kim and A. E. Herr. “Protein immobilization techniques for microfluidic assays”. In: *Biomicrofluidics* 7.4 (2013), p. 41501. ISSN: 1932-1058 (Print) 1932-1058 (Linking). DOI: 10.1063/1.4816934.
- [98] Joaquín Klug et al. “Chemical and Electrochemical Oxidation of Silicon Surfaces Functionalized with APTES: The Role of Surface Roughness in the AuNPs Anchoring Kinetics”. In: *The Journal of Physical Chemistry C* 117.21 (2013), pp. 11317–11327. ISSN: 1932-7447 1932-7455. DOI: 10.1021/jp212613f.

- [99] N. Lange et al. “New azidation methods for the functionalization of silicon nitride and application in copper-catalyzed azide-alkyne cycloaddition (CuAAC)”. In: *Surface and Interface Analysis* 48.7 (2016), pp. 621–625. ISSN: 01422421. DOI: 10.1002/sia.5950.
- [100] A. P. Le Brun et al. “The structural orientation of antibody layers bound to engineered biosensor surfaces”. In: *Biomaterials* 32.12 (2011), pp. 3303–11. ISSN: 1878-5905 (Electronic) 0142-9612 (Linking). DOI: 10.1016/j.biomaterials.2011.01.026.
- [101] Marco E. Marques, Alexandra A. P. Mansur, and Herman S. Mansur. “Chemical functionalization of surfaces for building three-dimensional engineered biosensors”. In: *Applied Surface Science* 275 (2013), pp. 347–360. ISSN: 01694332. DOI: 10.1016/j.apsusc.2012.12.099.
- [102] A. Psarouli et al. “Covalent Binding vs. Adsorption of Biomolecules on Silicon Nitride Planar Waveguides”. In: *Procedia Engineering* 25 (2011), pp. 350–353. ISSN: 18777058. DOI: 10.1016/j.proeng.2011.12.086.
- [103] P. Saengdee et al. “Optimization of 3-aminopropyltriethoxysilane functionalization on silicon nitride surface for biomolecule immobilization”. In: *Talanta* 207 (2020), p. 120305. ISSN: 1873-3573 (Electronic) 0039-9140 (Linking). DOI: 10.1016/j.talanta.2019.120305.
- [104] Shengwei Tan et al. “DNA-functionalized silicon nitride nanopores for sequence-specific recognition of DNA biosensor”. In: *Nanoscale Research Letters* 10.1 (2015). ISSN: 1556-276X. DOI: 10.1186/s11671-015-0909-0.
- [105] Thien Dien To et al. “Modification of silicon nitride surfaces with GOPES and APTES for antibody immobilization: computational and experimental studies”. In: *Advances in Natural Sciences: Nanoscience and Nanotechnology* 6.4 (2015). ISSN: 2043-6262. DOI: 10.1088/2043-6262/6/4/045006.
- [106] Patrick Vermette et al. “Immobilization and surface characterization of NeutrAvidin biotin-binding protein on different hydrogel interlayers”. In: *Journal of Colloid and Interface Science* 259.1 (2003), pp. 13–26. ISSN: 00219797. DOI: 10.1016/s0021-9797(02)00185-6.
- [107] Cláudia R. Vistas, Ana C. P. Águas, and Guilherme N. M. Ferreira. “Silanization of glass chips—A factorial approach for optimization”. In: *Applied Surface Science* 286 (2013), pp. 314–318. ISSN: 01694332. DOI: 10.1016/j.apsusc.2013.09.077.

- [108] Cuie Wang et al. "Different EDC/NHS Activation Mechanisms between PAA and PMAA Brushes and the Following Amidation Reactions". In: *Langmuir* 27.19 (2011), pp. 12058–12068. ISSN: 0743-7463 1520-5827. DOI: 10.1021/la202267p.
- [109] Meral Yüce and Hasan Kurt. "How to make nanobiosensors: surface modification and characterisation of nanomaterials for biosensing applications". In: *RSC Adv.* 7.78 (2017), pp. 49386–49403. ISSN: 2046-2069. DOI: 10.1039/c7ra10479k.
- [110] K. AbuZineh et al. "Microfluidics-based super-resolution microscopy enables nanoscopic characterization of blood stem cell rolling". In: *Sci Adv* 4.7 (2018), eaat5304. ISSN: 2375-2548 (Electronic) 2375-2548 (Linking). DOI: 10.1126/sciadv.aat5304.
- [111] Bruce Alberts et al. *Molecular Biology of the Cell*. ISBN: 0815345240.
- [112] Kai-Chien Chang and Daniel A. Hammer. "The Forward Rate of Binding of Surface-Tethered Reactants: Effect of Relative Motion between Two Surfaces". In: *Bioophysical Journal* 76.3 (1999), pp. 1280–1292. ISSN: 0006-3495. DOI: 10.1016/s0006-3495(99)77291-7.
- [113] Rui Cheng, Taotao Zhu, and Leidong Mao. "Three-dimensional and analytical modeling of microfluidic particle transport in magnetic fluids". In: *Microfluidics and Nanofluidics* 16.6 (2013), pp. 1143–1154. ISSN: 1613-4982 1613-4990. DOI: 10.1007/s10404-013-1280-z.
- [114] S. Choi et al. "A cell rolling cytometer reveals the correlation between mesenchymal stem cell dynamic adhesion and differentiation state". In: *Lab Chip* 14.1 (2014), pp. 161–6. ISSN: 1473-0189 (Electronic) 1473-0189 (Linking). DOI: 10.1039/c3lc50923k.
- [115] S. J. DeNardo et al. "Thermal dosimetry predictive of efficacy of 111In-ChL6 nanoparticle AMF-induced thermoablative therapy for human breast cancer in mice". In: *J Nucl Med* 48.3 (2007), pp. 437–44. ISSN: 0161-5505 (Print) 0161-5505 (Linking).
- [116] Benjamin Doffek. "Magnetic flow cytometry for thrombocyte analysis". Thesis. 2015.
- [117] M. Ermis, E. Antmen, and V. Hasirci. "Micro and Nanofabrication methods to control cell-substrate interactions and cell behavior: A review from the tissue engineering perspective". In: *Bioact Mater* 3.3 (2018), pp. 355–369. ISSN: 2452-

- 199X (Electronic) 2452-199X (Linking). DOI: 10.1016/j.bioactmat.2018.05.005.
- [118] Martin A. M. Gijs. "Magnetic bead handling on-chip: new opportunities for analytical applications". In: *Microfluidics and Nanofluidics* (2004). ISSN: 1613-4982 1613-4990. DOI: 10.1007/s10404-004-0010-y.
- [119] Cordula Grüttner et al. "Synthesis and antibody conjugation of magnetic nanoparticles with improved specific power absorption rates for alternating magnetic field cancer therapy". In: *Journal of Magnetism and Magnetic Materials* 311.1 (2007), pp. 181–186. ISSN: 03048853. DOI: 10.1016/j.jmmm.2006.10.1151.
- [120] U. Hassan et al. "A point-of-care microfluidic biochip for quantification of CD64 expression from whole blood for sepsis stratification". In: *Nat Commun* 8 (2017), p. 15949. ISSN: 2041-1723 (Electronic) 2041-1723 (Linking). DOI: 10.1038/ncomms15949.
- [121] M. Hejazian, W. Li, and N. T. Nguyen. "Lab on a chip for continuous-flow magnetic cell separation". In: *Lab Chip* 15.4 (2015), pp. 959–70. ISSN: 1473-0189 (Electronic) 1473-0189 (Linking). DOI: 10.1039/c4lc01422g.
- [122] Michael Helou et al. "Time-of-flight magnetic flow cytometry in whole blood with integrated sample preparation". In: *Lab on a Chip* 13.6 (2013). ISSN: 1473-0197 1473-0189. DOI: 10.1039/c3lc41310a.
- [123] Yu-Ching Hsiao et al. "Capturing magnetic bead-based arrays using perpendicular magnetic anisotropy". In: *Applied Physics Letters* 115.8 (2019). ISSN: 0003-6951 1077-3118. DOI: 10.1063/1.5085354.
- [124] Joseph J. Stupak Jr. "A METHOD OF CALIBRATING HELMHOLTZ COILS FOR THE MEASUREMENT OF PERMANENT MAGNETS". In: () .
- [125] Georgios Kokkinis et al. "Microfluidic platform with integrated GMR sensors for quantification of cancer cells". In: *Sensors and Actuators B: Chemical* 241 (2017), pp. 438–445. ISSN: 09254005. DOI: 10.1016/j.snb.2016.09.189.
- [126] J. M. Koo and C. Kleinstreuer. "Liquid flow in microchannels: experimental observations and computational analyses of microfluidics effects". In: *Journal of Micromechanics and Microengineering* 13.5 (2003), pp. 568–579. ISSN: 0960-1317. DOI: PiiS0960-1317(03)57671-9Doi10.1088/0960-1317/13/5/307.
- [127] H. G. Kye et al. "Dual-neodymium magnet-based microfluidic separation device". In: *Sci Rep* 9.1 (2019), p. 9502. ISSN: 2045-2322 (Electronic) 2045-2322 (Linking). DOI: 10.1038/s41598-019-45929-y.

- [128] Tongshu Li et al. "Study on the Characteristic Point Location of Depth Average Velocity in Smooth Open Channels: Applied to Channels with Flat or Concave Boundaries". In: *Water* 12.2 (2020). ISSN: 2073-4441. DOI: 10 . 3390 / w12020430.
- [129] Antonios Liakopoulos, Filippos Sofos, and Theodoros E. Karakasidis. "Friction factor in nanochannel flows". In: *Microfluidics and Nanofluidics* 20.1 (2016). ISSN: 1613-4982. DOI: 10 . 1007/s10404-015-1699-5.
- [130] F. Liu, L. Ni, and J. Zhe. "Lab-on-a-chip electrical multiplexing techniques for cellular and molecular biomarker detection". In: *Biomicrofluidics* 12.2 (2018), p. 021501. ISSN: 1932-1058 (Print) 1932-1058 (Linking). DOI: 10 . 1063 / 1 . 5022168.
- [131] H. Y. Liu et al. "Evaluation of Microfluidic Ceiling Designs for the Capture of Circulating Tumor Cells on a Microarray Platform". In: *Adv Biosyst* 4.2 (2020), e1900162. ISSN: 2366-7478 (Print) 2366-7478 (Linking). DOI: 10 . 1002/adbi . 201900162.
- [132] R. Liu et al. "Combinatorial Immunophenotyping of Cell Populations with an Electronic Antibody Microarray". In: *Small* 15.51 (2019), e1904732. ISSN: 1613-6829 (Electronic) 1613-6810 (Linking). DOI: 10 . 1002/smll . 201904732.
- [133] J. Loureiro et al. "Magneto resistive Detection of Magnetic Beads Flowing at High Speed in Microfluidic Channels". In: *IEEE Transactions on Magnetics* 45.10 (2009), pp. 4873–4876. ISSN: 0018-9464. DOI: 10 . 1109/tmag . 2009 . 2026287.
- [134] Masoud Madadelahi et al. "Mathematical modeling and computational analysis of centrifugal microfluidic platforms: a review". In: *Lab on a Chip* 20.8 (2020), pp. 1318–1357. ISSN: 1473-0197. DOI: 10 . 1039/c9lc00775j.
- [135] David Patrick McIntyre, Ali Lashkaripour, and Douglas Densmore. "Rapid and Inexpensive Microfluidic Electrode Integration with Conductive Ink". In: *Lab on a Chip* (2020). ISSN: 1473-0197 1473-0189. DOI: 10 . 1039/d0lc00763c.
- [136] A. Munaz, M. J. A. Shiddiky, and N. T. Nguyen. "Recent advances and current challenges in magnetophoresis based micro magnetofluidics". In: *Biomicrofluidics* 12.3 (2018), p. 031501. ISSN: 1932-1058 (Print) 1932-1058 (Linking). DOI: 10 . 1063/1 . 5035388.
- [137] Nam-Trung Nguyen. "Micro-magnetofluidics: interactions between magnetism and fluid flow on the microscale". In: *Microfluidics and Nanofluidics* 12.1-4 (2011), pp. 1–16. ISSN: 1613-4982 1613-4990. DOI: 10 . 1007/s10404-011-0903-5.

- [138] N. Pamme. "Magnetism and microfluidics". In: *Lab Chip* 6.1 (2006), pp. 24–38. ISSN: 1473-0197 (Print) 1473-0189 (Linking). DOI: 10.1039/b513005k.
- [139] Jan Walther Perthold and Chris Oostenbrink. "Simulation of Reversible Protein–Protein Binding and Calculation of Binding Free Energies Using Perturbed Distance Restraints". In: *Journal of Chemical Theory and Computation* 13.11 (2017), pp. 5697–5708. ISSN: 1549-9618 1549-9626. DOI: 10.1021/acs.jctc.7b00706.
- [140] Anne Pierres et al. "Dissecting Streptavidin-Biotin Interaction with a Laminar Flow Chamber". In: *Biophysical Journal* 82.6 (2002), pp. 3214–3223. ISSN: 0006-3495. DOI: 10.1016/s0006-3495(02)75664-6.
- [141] Mathias Reisbeck et al. "Magnetic fingerprints of rolling cells for quantitative flow cytometry in whole blood". In: *Scientific Reports* 6.1 (2016). ISSN: 2045-2322. DOI: 10.1038/srep32838.
- [142] Julian Schütt et al. "Two Orders of Magnitude Boost in the Detection Limit of Droplet-Based Micro-Magnetofluidics with Planar Hall Effect Sensors". In: *ACS Omega* 5.32 (2020), pp. 20609–20617. ISSN: 2470-1343 2470-1343. DOI: 10.1021/acsomega.0c02892.
- [143] Julian Schütt et al. "Nanocytometer for smart analysis of peripheral blood and acute myeloid leukemia: a pilot study". In: *Nano Letters* (2020). ISSN: 1530-6984 1530-6992. DOI: 10.1021/acs.nanolett.0c02300.
- [144] F. Shamsipour et al. "Conjugation of Monoclonal Antibodies to Super Paramagnetic Iron Oxide Nanoparticles for Detection of her2/neu Antigen on Breast Cancer Cell Lines". In: *Avicenna J Med Biotechnol* 1.1 (2009), pp. 27–31. ISSN: 2008-2835 (Print) 2008-2835 (Linking).
- [145] S. S. Shevkoplyas et al. "The force acting on a superparamagnetic bead due to an applied magnetic field". In: *Lab Chip* 7.10 (2007), pp. 1294–302. ISSN: 1473-0197 (Print) 1473-0189 (Linking). DOI: 10.1039/b705045c.
- [146] Christian Sommer. "Die Größenabhängigkeit der Gleichgewichtsgeschwindigkeit von Partikeln beim Transport in Mikrokanälen". Thesis. 2014.
- [147] Daoyun Song, Rakesh K. Gupta, and Rajendra P. Chhabra. "Drag on a Sphere in Poiseuille Flow of Shear-Thinning Power-Law Fluids". In: *Industrial and Engineering Chemistry Research* 50.23 (2011), pp. 13105–13115. ISSN: 0888-5885 1520-5045. DOI: 10.1021/ie102120p.

- [148] H. C. Tekin, M. Cornaglia, and M. A. Gijs. “Attomolar protein detection using a magnetic bead surface coverage assay”. In: *Lab Chip* 13.6 (2013), pp. 1053–9. ISSN: 1473-0189 (Electronic) 1473-0189 (Linking). DOI: 10.1039/c3lc41285g.
- [149] A. E. Urusov et al. “Rapid immunoenzyme assay of aflatoxin B1 using magnetic nanoparticles”. In: *Sensors (Basel)* 14.11 (2014), pp. 21843–57. ISSN: 1424-8220 (Electronic) 1424-8220 (Linking). DOI: 10.3390/s141121843.
- [150] C. Wang et al. “A novel wide-range microfluidic dilution device for drug screening”. In: *Biomicrofluidics* 13.2 (2019), p. 024105. ISSN: 1932-1058 (Print) 1932-1058 (Linking). DOI: 10.1063/1.5085865.
- [151] Haoli Wang and Yuan Wang. “Measurement of water flow rate in microchannels based on the microfluidic particle image velocimetry”. In: *Measurement* 42.1 (2009), pp. 119–126. ISSN: 02632241. DOI: 10.1016/j.measurement.2008.04.012.
- [152] Hitoshi Watarai and Makoto Namba. “Capillary magnetophoresis of human blood cells and their magnetophoretic trapping in a flow system”. In: *Journal of Chromatography A* 961.1 (2002), pp. 3–8. ISSN: 00219673. DOI: 10.1016/s0021-9673(02)00748-3.
- [153] R. Wirix-Speetjens et al. “A force study of on-chip magnetic particle transport based on tapered conductors”. In: *IEEE Transactions on Magnetics* 41.10 (2005), pp. 4128–4133. ISSN: 0018-9464. DOI: 10.1109/tmag.2005.855345.
- [154] Tadayuki Yago et al. “Catch bonds govern adhesion through L-selectin at threshold shear”. In: *Journal of Cell Biology* 166.6 (2004), pp. 913–923. ISSN: 1540-8140. DOI: 10.1083/jcb.200403144.
- [155] Ryuji Yokokawa et al. “FORCE MEASUREMENT AND MODELING FOR MOTOR PROTEINS BETWEEN MICROSPHERE AND MICROFLUIDIC CHANNEL SURFACE”. In: ISBN: 978-0-9798064-3-8.
- [156] Taotao Zhu et al. “Analytical model of microfluidic transport of non-magnetic particles in ferrofluids under the influence of a permanent magnet”. In: *Microfluidics and Nanofluidics* 10.6 (2011), pp. 1233–1245. ISSN: 1613-4982 1613-4990. DOI: 10.1007/s10404-010-0754-5.
- [157] Nora Graf et al. “Optimization of cleaning and amino- silanization protocols for Si wafers to be used as platforms for biochip microarrays by surface analysis (XPS, ToF-SIMS and NEXAFS spectroscopy)”. In: *Surface and Interface Analysis* 40.3-4 (2008), pp. 180–183. ISSN: 0142-2421. DOI: 10.1002/sia.2621.

- [158] James V. Staros. "N-hydroxysulfosuccinimide active esters: bis(N-hydroxysulfosuccinimide) esters of two dicarboxylic acids are hydrophilic, membrane-impermeant, protein cross-linkers". In: *Biochemistry* 21.17 (1982). PMID: 7126526, pp. 3950–3955. DOI: 10.1021/bi00260a008.
- [159] A.F. Stalder et al. "A Snake-Based Approach to Accurate Determination of Both Contact Points and Contact Angles". In: *Colloids And Surfaces A: Physicochemical And Engineering Aspects* 286.1-3 (Sept. 2006), pp. 92–103.
- [160] Johannes Schindelin et al. "Fiji: an open-source platform for biological-image analysis". In: *Nature Methods* 9.7 (2012), pp. 676–682. ISSN: 1548-7091. DOI: 10.1038/nmeth.2019.
- [161] Yael Eisenberg-Domovich et al. "High-resolution crystal structure of an avidin-related protein: insight into high-affinity biotin binding and protein stability". In: *Acta Crystallographica Section D* 61.5 (May 2005), pp. 528–538. DOI: 10.1107/S0907444905003914.

Statement

I declare that I have authored this thesis independently, that I have not used other than the declared sources / resources, and that I have explicitly marked all material which has been quoted either literally or by content from the used sources.

Munich, December 4th, 2020, Signature